Title
Mathematical Models of Vaccine-Preventable Disease in California

Author
Ackley, Sarah F

Publication Date
2018

Peer reviewed|Thesis/dissertation

Mathematical Models of Vaccine-Preventable Disease in California

by

Sarah F. Ackley

DISSERTATION

Submitted in partial satisfaction of the requirements for the degree of

DOCTOR OF PHILOSOPHY

in

Epidemiology and Translational Sciences

in the

GRADUATE DIVISION

of the

UNIVERSITY OF CALIFORNIA, SAN FRANCISCO

Dedication and Acknowledgments

I would first and foremost like to thank my PhD advisor and dissertation chair, Professor Travis C. Porco. I would also to thank my other dissertation committee members: Professors Maria Glymour and James Lloyd Smith. I would also like to thank a number of other professors who have played a role in mentoring me during my time at UCSF: Caitlin S. Pepperell, Thomas M. Lietman, George Rutherford, Adam Bennett, and Robert Hiatt.

I would like to thank my classmates, and in particular my cohort: Caroline Tai, Kathryn Ray, Tu My To, and Kristen Aiemjoy. I would also like to thank current and former members of of the Porco research group: Lee Worden, Rae Wannier, Wayne Enanoria, and Fengchen Liu.

I would like to acknowledge my collaborators, without whom this work would not be possible. From the California Department of Public Health Immunizations Branch, I would like to in particular thank Drs. Jennifer Zipprich, Erin Murray, and Kathleen Harriman. From Kinsa, Inc., I would like to thank Sarah Pilewski and Dr. Vladimir S. Petrovic.

I would also like to acknowledge the PhD Program in Epidemiology, the Department of Epidemiology and Biostatistics, the Proctor Foundation, as well as my funding sources: the NIGMS MIDAS Program (F31GM120985 & U01GM087728) and the Achievement Rewards for College Scientists (ARCS) Foundation.

Acknowledgment of Previously Published Materials

A version of Chapter 1 of this dissertation has been published in *Clinical Infectious Diseases* (see full citation below). The published material is substantially the product of Sarah F. Ackley's period of study at UCSF and was primarily conducted and written by her. The work she completed for this published manuscript is comparable to a standard dissertation chapter.

Approved: 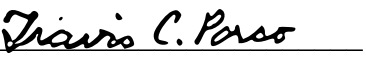 Travis C. Porco, PhD, MPH, Dissertation Chair

Sarah F Ackley, Jill K Hacker, Wayne T A Enanoria, Lee Worden, Seth Blumberg, Travis C Porco, Jennifer Zipprich; Genotype-Specific Measles Transmissibility: A Branching Process Analysis, *Clinical Infectious Diseases*, Volume 66, Issue 8, 3 April 2018, Pages 1270–1275, https://doi.org/10.1093/cid/cix974.

Mathematical Models of Vaccine-Preventable Disease in California

Sarah F. Ackley

Abstract

In chapter 1, using a Galton-Watson branching-process analysis, we characterize differences in measles transmission by estimating the association between genotype and the reproduction number among post-elimination California measles cases. Genotype B3 is found to be a significant predictor of transmissibility.

In chapter 2, we determine whether data from FDA-cleared wired and Bluetooth *smart* thermometers sold by a San Francisco-based company aid influenza forecasting efforts. We compare this *smart thermometer* data to regional influenza and ILI surveilance data from the California Department of Public Health. We evaluated the correlation between the regional California surveillance data and smart thermometer data, tested the hypothesis that smart thermometer readings and symptom reports provide regionally specific predictions, and determined whether smart thermometer and mobile application improved disease forecasts. Our results are consistent with the hypothesis that smart thermometer readings and symptom reports reflect underlying disease transmission in California. Data from such cloud-based devices could supplement syndromic influenza surveillance data.

In chapter 3, we examine whether changes in varicella transmissibility may have occurred following the change from one- to two-dose vaccination scheduling in 2007. Following the change in ACIP recommendations for varicella vaccination in 2007, the median outbreak size decreased. However, while the number of outbreaks has continued to decrease following 2008, we do not find evidence that the distribution of sizes has changed since 2008. Using insights from branching process models assuming both subcritical and supercritical transmission and with and without

depletion of susceptibles, we cannot rule out that varicella transmission is supercritical in school-based settings.

Table of Contents

List of Tables

List of Figures

Chapter 1

Genotype-Specific Measles Transmissibility: A Branching Process Analysis

Introduction

As a result of a successful measles vaccination program in the United States, measles was declared eliminated in 2000 (Orenstein et al. (2004), Katz et al. (2004)). Measles elimination is defined as the absence of continuous measles transmission for 12 months or more in a defined geographic area (Fiebelkorn et al. (2010)). However, measles remains a significant public health concern as measles importations continue to occur resulting in limited outbreaks, small clusters or transmission chains. While the number of measles cases continues to increase nationally, there's no direct evidence of difference in susceptible populations over the time period included in our study. Therefore, this trend may be due to an increase in the number of disease introductions rather than a change in levels of population immunity (Blumberg, Enanoria, et al. (2014)).

In California, 400 measles cases were reported from January 1, 2000 through December 31, 2015. The December 2014 to March 2015 measles outbreak linked to Disneyland theme parks was the largest outbreak in California since elimination, with 131 California cases, 16 cases in other states, 159 cases in a religious community in Quebec, Canada, and one case in Mexico (Zipprich et al. (2015), Blumberg, Worden et al. (2015)). The majority of the California cases were unvaccinated or had unknown vaccination status; organized opposition to vaccination, the key component of measles control, remains a significant concern (Mello et al. (2015)). In addition, the outbreak linked to Disneyland theme parks is consistent with an effective reproduction number that is unchanged from the 2001-2011 era (Blumberg, Worden et

al. (2015), Blumberg, Enanoria, et al. (2015)), indicating that the level of population immunity may have remained roughly constant since elimination.

There may be alternative explanations for why some measles outbreaks are larger. The World Health Organization (WHO) recognizes 8 clades of measles virus, within which there are 24 recognized genotypes, of which six are currently circulating (Coughlin et al. (2017)). Measles clade B viruses (genotypes B1, B2, B3) are endemic to sub-Saharan Africa; prior to 2010, genotype B3 had been associated with frequent importations from African counties (Rota et al. (2011)). Following a measles genotype B3 outbreak in the Philippines in 2014, genotype B3 has been detected in all six WHO regions (Rota et al. (2016)). The 2014-2015 outbreak linked to Disneyland theme parks was an outbreak attributed to genotype B3 (Zipprich et al. (2015)), and the CDC determined that the strain of B3 identified in this outbreak was identical to the strain associated with the Philippines outbreak (CDC, Measles Cases & Outbreaks). The global distribution of the measles genotype B3 appeared to expand dramatically after the Philippines outbreak and was associated with in record numbers of US measles cases in both 2014 and 2015.

These observations prompted consideration of whether there might be genotype-specific differences in measles transmission. Our analysis aimed to characterize differences in measles transmission by estimating the association between genotype and effective reproduction number among post-elimination California measles cases. We also evaluated whether other variables collected during routine surveillance such as season of introduction and age and vaccine status of the index case may confound this relationship.

Methods

Terms

For conciseness, we use outbreak to refer to clusters of size two and isolated cases, as well as clusters large enough to meet the CDC definition of outbreak (three or more epidemiologically linked cases in space and time (CDC (2016)). Isolated cases are part of a transmission chain where the source case(s) is either not identified or may be known but was reportable outside of the jurisdiction of California. We use index case to refer to the progenitor case or cases, and also note that this differs from the CDC definition of the first identified case, who may be later in the transmission chain. We use R to refer to the reproduction number under vaccination (Scherer et al. (2002)). Lastly, for clarity, we use outbreak A to refer to the transmission that occurred outside of Disneyland theme parks during the 2014-15 California outbreak linked to Disneyland theme parks, since the nature of the transmission events that occurred at Disneyland theme parks is unknown (Blumberg, Worden et al. (2015)). See additional details under *Case Ascertainment*.

Case Ascertainment

Reported measles cases that met the Council of State and Territorial Epidemiologists (CSTE) case definition for confirmed measles were included in the analysis. For the majority of outbreaks, the case with the earliest rash onset date was considered the only index case for the outbreak. Additional outbreaks include two outbreaks with 2 and 3 contemporaneous cases, in which all were considered index cases, and outbreak A. For the latter outbreak, the case or cases who transmitted at Disneyland theme parks were never identified. Therefore, 42 cases who visited Disneyland theme parks during a three-day period and three additional cases whose rash onset dates were consistent with acquiring infection during that three-day period were all

considered index cases for that outbreak. The undocumented, extreme transmission event(s) that resulted in this large number of secondary cases that occurred at or near Disneyland theme parks was omitted; only the subsequent known transmission, which likely is more typical of transmission in California (Blumberg, Worden et al. (2015)), has been included in the estimation of the reproduction number.

Genetic Characterization

Measles virus genotypes were determined using a 450 nucleotide sequence of the nucleoprotein gene (N-450) at either the California Department of Public Health (CDPH) Viral and Rickettsial Disease Laboratory (VRDL) or the Centers for Disease Control and Prevention (CDC) Measles Virus Laboratory (WHO (2015)). Outbreaks were assigned the genotype corresponding to any individual or individuals with epidemiologic linkage in that outbreak for whom genotyping was performed.

Analysis

Branching process theory (Harris (1963)) has been used to estimate the reproduction numbers of many subcritical diseases (Farrington et. al (2003), Lloyd-Smith et al. (2005)). Prior work on branching process models has outlined the approach to fitting multi-genotype models that we propose for this research. (For example, Blumberg, Funk et al. (2014) fits a model with two reproduction numbers.) The secondary case distribution gives is the probability distribution of the number of secondary cases per case in a branching process model (Blumberg, Funk et al. (2014)). Specifically, assuming a negative binomial secondary case distribution, a mathematical expression for the distribution of outbreak sizes can be derived (see Blumberg, Worden et al.

(2015) & Blumberg, Funk et al. (2014)) and is employed in our analysis. A negative binomial secondary case distribution is preferable to the limiting Poisson or geometric distributions, because it yields an empirically better fit to data (Lloyd-Smith et al. (2005)) and accounts for heterogeneity in transmissibility (Blumberg et al. (2013)).

Assuming a negative binomial secondary case distribution, a closed-form solution is available for the distribution of outbreak sizes when transmission is subcritical (Blumberg, Funk et al. (2014), Nishiura et al. (2015)). The closed-form solution for the distribution of outbreak sizes can be found elsewhere (Blumberg, Worden et al. (2015), Blumberg et al. (2013)) and is a function of the number of index cases; R, the mean of the secondary case distribution; and k, the dispersion parameter, a measure of heterogeneity in transmission, with smaller values indicative of a larger variance in the secondary case distribution. ($k = 1$ corresponds to a geometric secondary case distribution and $k = \infty$ corresponds to a Poisson distribution.) Fitting this model to the distri- bution of outbreak sizes using maximum likelihood, we can estimate the reproduction number R (Blumberg, Funk et al. (2014)).

Exact p-values for heterogeneity across genotype and other predictors were determined using permutation tests (1,024 permutations) to determine the probability of seeing a ratio of reproduction numbers larger than was observed. Confidence intervals for reproduction numbers were obtained by percentile bootstrap (1,024 replicates). A type I error rate of 0.05 was used to test the hypothesis that genotype B3 is more transmissible than other genotypes.

It is possible that out of many genotypes one genotype would appear to give rise to larger outbreaks by chance, and in testing this genotype against all others we would be susceptible to the Texas sharpshooter fallacy (Nuzzo (2015)). To address this, we performed an additional sensitivity analysis in which we analyze the data using a multi-genotype model. Specifically, we

used a random-effect model to model a random effect for transmissibility by genotype. We used the distribution of outbreak sizes in equation 1, where the *logit* of the reproduction number *R* varies by genotype and is sampled from a normal distribution with variance σ^2. The probability of the observed outbreaks of a given genotype for this model is the following:

$$\Pr(\mathbf{Y}) = \prod_{g=1}^{G} \int_{R=0}^{R=1} \prod_{i=1}^{N_g} \Pr(Y_{i,g}|R,k) f(R,\mu,\sigma) dR \tag{1}$$

where **Y** is a vector of all observed outbreak sizes, *G* is the total number of observed genotypes, *g* is a specific genotype, N_g is the number of outbreaks of genotype *g*, $Y_{i,g}$ is the size of the *i*th outbreak of genotype *g*, and $f(R,\mu,\sigma) = \frac{1}{\sqrt{2\pi\sigma^2}} \frac{1}{R(1-R)} \exp\left(-\frac{(\text{logit}R-\mu)^2}{2\sigma^2}\right)$. We then maximized the likelihood with respect to μ and σ and performed a likelihood ratio test with a model with σ equal to zero, adjusting for the fact that the null hypothesis is on the boundary (Fitzmaurice et. al (2012)). We perform a similar analysis with season of outbreak.

Results

There were 400 measles cases and 165 outbreaks in California from January 1, 2000 to December 31, 2015. Table 1.1 summarizes the genotype data available for this study. For 2000-2015, we estimate the overall reproduction number to be 0.47, 95% confidence interval: (0.31, 0.55). Permutation p-values for the effect of genotype, season of introduction, age of the index case, vaccine status of the index are given in Table 1.2. Since we find compelling evidence that genotype and age of the index case are significant predictors of measles transmissibility, we present effect estimates and confidence intervals in Table 1.3. These effect estimates are also summarized in Figure 1.1. (Parameter estimates for the random effect models are given in Table 1.S1 and estimated dispersion parameters are given in Table 1.S3.)

Genotype	Total Cases, (Excluding Outbreak A)	Number of Outbreaks, (Excluding Outbreak A)	Mean Outbreak Size, (Excluding Outbreak A, per Index Case)
B3	183, (52)	21, (20)	8.71, (2.6, 2.61)
D3	4	2	2
D4	23	16	1.44
D5	16	3	5.33
D6	3	2	1.5
D7	12	4	3
D8	42	28	1.5
D9	14	8	1.75
G2	5	1	5
H1	8	8	1
No Genotype	90	72	1.25, (1.25, 1.2)
Total	400, (269)	165, (164)	2.42, (1.64, 1.62)

Table 1.1: California measles cases since elimination: case counts, number of out- breaks, and mean outbreak size by genotype that include and exclude outbreak A. Values for excluding outbreak A or per index case outbreak sizes are given in parentheses only when these values differ from the value including outbreak A.

Variable	p-value (Including outbreak A)	p-value (Excluding outbreak A)	p-value (Outbreaks with One Index Case)
Genotype (B3 vs. not)	0.01	0.04	-
Season of introduction (winter vs. not)	0.01	0.03	-
Age of index Case (school-aged vs. not)	-	-	< 0.001
Vaccine status of index case (vaccinated vs. unvaccinated or unknown status)	-	-	0.12
Random Effect of Genotype*	0.004	0.02	-
Random Effect of Season*	0.14	0.42	-

Table 1.2: p-values for various predictors of measles transmissibility. Starred p-values are χ^2 likelihood ratio p-values. All other p-values are permutation p-values.

	Reproduction Number R (95% CI)
Overall	0.47 (0.31,0.55)
B3	0.64 (0.48,0.71)
Non-B3	0.43 (0.28,0.54)
School-Aged	0.69 (0.52,0.78)
Non-School Aged	0.28 (0.19,0.35)

Table 1.3: Estimated reproduction numbers for measles transmission: overall (all outbreaks), genotype B3 vs. non-B3 genotypes (only for genotyped outbreaks), and school-aged (ages 5-18 years) vs. non-school aged (only for outbreaks with a single index case). Dispersion parameters were estimated and are included in the Supplemental Information.

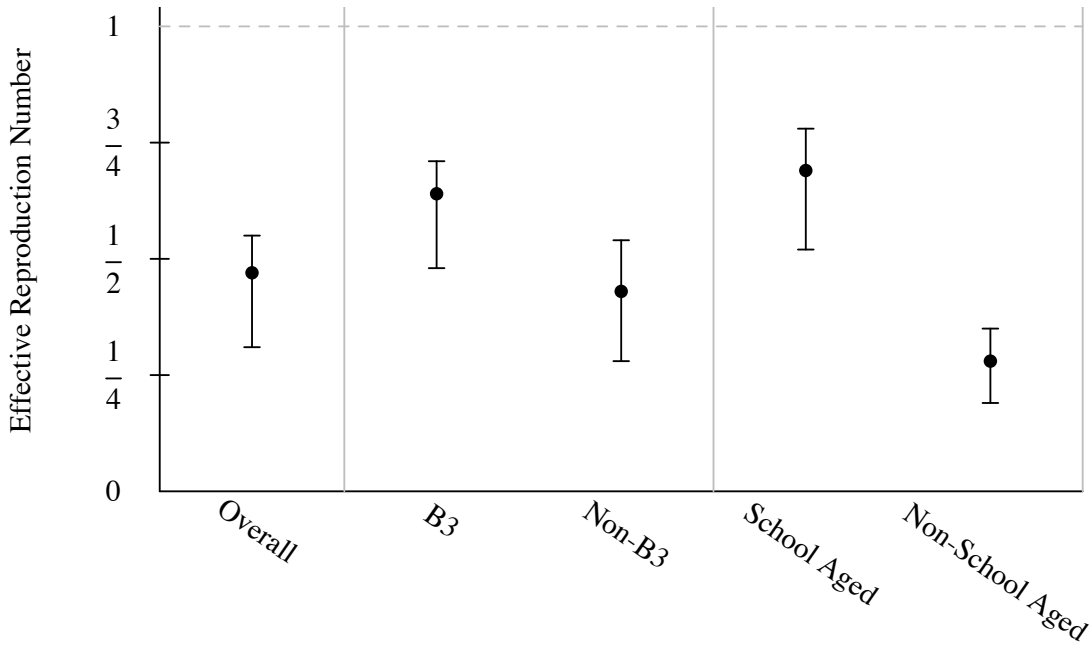

Figure 1.1: Estimated reproduction numbers for measles transmission: overall, genotype B3 vs. non-B3 genotypes, and school-aged (age 5-18 years) vs. non-school aged index cases.

Discussion

We evaluated whether or not differences between genotypes may be responsible for differences in observed outbreak sizes and measles transmissibility. Genotype is significantly associated with transmissibility, irrespective of type of analysis (Table 1.2). Prior studies (Blumberg, Worden et al. (2015), Blumberg, Enanoria et al. (2015), Majumder et al. (2015)) have indicated that there is not compelling evidence for declining population immunity over time during the elimination era, so we evaluated other plausible confounders in the relationship between genotype and outbreak size. Since a significant number of index cases were US residents with recent international travel, season of introduction is plausibly associated with genotype: travel to areas with circulating B3 strains might be more common in the cooler winter months. (Table 1.S2 in the Supplemental Information shows that it does appear that the fraction of winter B3 introductions is greater than that of other seasons.) However, while season appears significantly associated with transmissibility when comparing the winter season to all other seasons, in a random effect model the effect of season is nonsignificant. We think it is unlikely that age of index case or vaccine status of the index case are causally related to infecting viral genotype (see Supplemental Information for more information). However, school-age appears to be a significant predictor of measles transmissibility, likely due to the number of contacts (Mikolajczyk et al. (2008)) and the potential clustering based on vaccination status, particularly among household contacts (Sugerman et al. (2015)).

Contact investigations may have several decision points, and a better understanding of predictors of transmission could be used minimize transmission. While routine vaccination remains the most important control measure for measles, other control measures such as home quarantine and post-exposure prophylaxis (PEP) are an important part of the on-the-ground

response during an outbreak (Liu et al. (2015)). Contact investigations for measles and delivering PEP to susceptible contacts of cases are resource intensive and divert funds and staff resources from other public health programs (Dayan et al. (2004), Ortega-Sanchez et al. (2011)). Thus, it would be advantageous to have a marker of transmissibility that could be used to focus public health efforts particularly in a setting of multiple cases and contact investigations competing for limited resources (Liu et al. (2015)). More accurately anticipating the number of cases during an outbreak could help improve resource and staff allocation.

Our results are consistent with prior analyses of California and US measles outbreaks. The previous estimate for the *R* for measles in the US between 2001 and 2011 is 0.52 (95% CI: 0.44, 0.60) (Blumberg et al. (2013)), consistent with an overall *R* for California from 2000-2015 of 0.47 (95% CI: 0.31, 0.55) estimated here. The prior estimate for the *R* for outbreak A is 0.69 (95% CI: 0.48, 1.04) (Blumberg, Worden et al. (2015)) (note this estimate assumed 40 index cases), consistent with an *R* of 0.64 (95%CI: 0.48, 0.71) estimated here for B3 strains. While in Blumberg, Worden et al. (2015) the *R* for outbreak A was not statistically significantly higher than the *R* for the 2001-2011 time period (which includes outbreaks of the B3 and non- B3 genotypes), the point estimate was higher, which is consistent with the hypothesis that B3 strains are more transmissible.

This study has several strengths. Measles has been widely studied using a variety of mathematical epidemiology techniques since the 1950s (Bailey (1953), Bartlett (1960), Measles (1957), Fine et al. (1982), Grenfell et al. (1992), Lloyd-Smith et al. (2005)). While pre-elimination era measles was characterized by continuous transmission with seasonal patterns in transmission (Fine et al. (1982)), measles transmission in the US is now characterized by small outbreaks following importation (Fiebelkorn et al. (2010)). Branching processes are ideal for

analyzing diseases that occur as isolated cases, transmission chains, and make it possible to determine whether changes in case counts are due to changes in transmissibility or changes in the numbers of introductions (Blumberg et al. (2013)). Thus, post-elimination era dynamics favor the branching process approach we employed (Farrington et al. (2013), Blumberg et al. (2013)).

In addition, we performed several sensitivity analyses to avoid the Texas sharpshooter fallacy (Nuzzo (2015)). Since outbreak A was the largest outbreak in California since elimination, this may have garnered increased, and perhaps undue, interest in the causal effects of genotype B3 and winter season on measles transmissibility. To address this possible fallacy, we omitted outbreak A and recalculated permutation p-values for all predictors of interest and analyzed genotype and season as a random effect. Our result that genotype is a predictor of transmissibility was robust to inclusion or exclusion of the outbreak A and random effects modeling. However, the effect of season is more questionable given that the p-value was significant when comparing winter to all other seasons, but not in a random-effect model. Lastly, for outbreak A, we only included known transmission events which occurred outside of the Disneyland theme parks; this transmission was likely more typical of transmission in California (Blumberg, Worden et al. (2015)). In addition, if there had been a known single index case, the decision to model this outbreak as an outbreak with 45 index cases effectively reduced our statistical power to detect a difference between B3 and non-B3 genotypes; given that we did detect a significant effect, this lends credibility to the hypothesis that there are genotype-specific differences in transmissibility. We note that the number of index cases we use has been updated and thus differs from the 40 used in Blumberg, Worden et al. (2015).

A weakness of this study is that we were limited by the number of California measles cases since elimination and thus the study may have been underpowered to detect significant

effects for key predictors. For example, in only 16 out of 163 single-index-case outbreaks was the index case vaccinated (the remainder had unknown vaccination status or were unvaccinated). While these outbreaks were on average characterized by less transmission, we did not detect a significant effect. In addition, we cannot distinguish between biological differences between genotypes (e.g. greater viral replication in the lungs for B3 strains (El Mubarak et al. (2007))) and differences in networks in which specific genotypes may tend to circulate (e.g. a larger number of contacts in networks where B3 strains tend to be introduced). While we would argue that biological differences between genotype B3 and other genotypes are plausible (El Mubarak et al. (2007)), since we did not include all possible confounders, our models cannot necessarily distinguish between competing explanations for differing transmissibility. While measles case ascertainment is thought to be high, missed cases are a possibility and could result in collider (selection) bias. For this to bias the observed association between genotype and outbreak in the observed direction, the B3 genotype would have to cause less severe disease. (Case detection would be enhanced, not diminished during large outbreaks.) While this would be at odds with El Mubarak et al. (2007), the B3 genotype could cause less severe disease if the measles vaccine were less effective against this genotype. (That is, genotype-B3 cases would be enriched with vaccinated and thus partially protected individuals compared with other outbreaks.) In addition, if the B3 genotype causes more severe disease, it is possible that B3 outbreaks would appear larger due to improved case finding. While we cannot rule out that genotype-B3 out- breaks appear larger because genotype B3 causes more severe disease with available data, the apparent public health impact of the B3 genotype nonetheless appears to be greater than that of other genotypes.

In conclusion, we have found that genotype appears to be a significant predictor of

measles transmissibility, with genotype B3 being more transmissible compared with all other genotypes combined. School age also appears to be a significant predictor of transmissibility. While we do not find compelling evidence that the relationship between genotype B3 and outbreak size is confounded by other factors, is remains to be seen whether this result could be replicated in other highly vaccinated populations. Furthermore, outbreak sizes are variable and, for example, genotype-B3 outbreaks will overlap substantially in size with non-B3 outbreaks. Thus, more data is needed before one could make a firm recommendation that genotype or age of index case could be used for guiding contact investigation. The view that non-B3 outbreaks or outbreaks with index cases not of school age are of lesser public health importance is unwarranted. While high levels of population immunity achieved through routine measles vaccination remains the cornerstone of control, variability in measles transmissibility may nonetheless have important implications for measles control: the vaccination threshold required for elimination may not be the same for all genotypes or age groups.

Chapter 1 Supplemental Information

Mixed Effect Models

Variable	Including Outbreak A: R, σ, k	Excluding Outbreak A: R, σ, k
Random Effect of Genotype	0.44, 0.9, >1000	0.43, 0.86, 11.86
Random Effect of Season	0.4, 0.46, 0.54	0.37, 0.18, 0.6

Table 1.S1: Random Effect Models: Estimated detransformed reproduction number *R*, standard deviation σ of logit *R*, and dispersion parameter *k*.

Plausibility of Association between Season and Genotype

Season	Number of Introductions	Proportion B3
Fall	14	0.20
Spring	47	0.11
Summer	40	0.06
Winter	64	0.38

Table 1.S2: Number of introductions and proportion of B3 introductions by season of introduction. The *p*-value for the association between genotype and season of introduction is 0.01 (Fisher's exact test).

Estimated Dispersion Parameters

	Reproduction Number R (95% CI)	Dispersion Parameter k (95% CI)
Overall	0.47 (0.31,0.55)	0.4 (0.19,1.99)
B3	0.64 (0.48,0.71)	19.51 (0.59, >1000)
Non-B3	0.43 (0.28,0.54)	
School-Aged	0.69 (0.52,0.78)	4.61 (0.49, >1000)
Non-School Aged	0.28 (0.19,0.35)	

Table 1.S3: Estimated reproduction numbers and dispersion parameters for measles transmission: overall (all outbreaks), genotype B3 vs. non-B3 genotypes (only for genotyped outbreaks), and school-aged (ages 5-18 years) vs. non-school aged (only for outbreaks with a single index case). Large dispersion parameters ($k > 1000$) are omitted for clarity; in such cases, the secondary case distribution is not distinguishable from a Poisson distribution.

Plausibility of Association between Age of Index Case and Genotype B3

Restricting to Index Cases of Outbreaks with a Single Index Case

Among B3 outbreaks with a single index case, 5 have a school-aged index case, while 15 do not. Among genotyped non-B3 outbreaks with a single index case, 8 have a school-aged index case, while 65 do not. The p-value for the association between school-age of index case and B3 genotype is 0.15 (Fisher's exact test).

Including All Index Cases

Including outbreaks with more than one index case (e.g. outbreak A), among B3 index cases, 11 were school-aged while 54 were not. Among index cases of genotyped non-B3 outbreaks, 8 where school-aged while 65 were not. The p-value for the association between school-age of index case and B3 strain is 0.33 (Fisher's exact test). Lastly, in outbreak A, 6 of the 45 index cases where school-aged (13.3%). This proportion is close to the proportion in the entire dataset: 30 out of 212 total index cases were school-aged (14.2%).

Chapter 2

Assessing the Utility of a Smart Thermometer and Mobile Application as a Surveillance Tool for Influenza and Influenza-Like Illness

Introduction

Participatory surveillance systems, or systems that encourage the general public to voluntarily report health-related information, have the potential to strengthen disease surveillance systems and provide realtime estimates of disease burden (Wójcik et al. (2014)). Influenza and influenza-like illnesses (ILIs) are significant public health concerns, but the timing and peak intensity vary considerably from season to season and regionally. Prediction of influenza and ILI trends could be used to help plan and execute an effective public health response (Biggerstaff et al. (2016)). In addition, delays in obtaining surveillance data have garnered interest in nowcasting, or the use of forecasting techniques to estimate current influenza and ILI activity (Lampos et al. (2015)). Kinsa, Inc. sells FDA-cleared Bluetooth and wired thermometers nationally and internationally. These *smart thermometers* synchronize with a mobile application, which records temperature readings and can also be used to record symptoms. Although multiple individuals, typically members of the same household, may share a thermometer, users may indicate which temperature readings and symptom reports belong to a specific user.

The potential for participatory surveillance for monitoring ILI has been explored in other settings (e.g. Smolinski et al. (2015), Marquet et al. (2006), Ortiz et al. (2011)) and in-the-field thermometers have been used for disease monitoring in school children in China (Hswen et al. (2017)). Previous work has shown that smart thermometer readings from the Kinsa application

can improve ILI forecasts using national CDC data (Miller et al. (2018)), and we aim to extend this work for influenza and smaller geographic regions. Given the use of an FDA-cleared thermometer with 33,000 users in California, the data collected from temperature readings and user-provided symptom reports from the Kinsa application may be informative for influenza forecasting efforts. Using California influenza laboratory surveillance data and ILI surveillance data from the 2015-16 and 2016-17 influenza seasons, we aim to determine whether the smart thermometer readings and symptom reports provide timely and regionally specific information on influenza and ILI trends. There is no standardized approach for simultaneously validating crowdsourced data and data from cloud-based devices. We therefore adopted a three-tiered approach to evaluate how the smart thermometer and mobile application data corresponded with California influenza surveillance data. First, we evaluated the correlation between the California influenza surveillance data and smart thermometer data. Second, we test the hypothesis that smart thermometer and mobile application data from a given season and region predicts influenza and ILI surveillance data for that season and region better than data from other seasons and regions. Lastly, in the most demanding test, we evaluate whether data from the smart thermometer and mobile application may be useful in influenza and ILI nowcasting and prediction efforts.

Methods

California Influenza Surveillance Data

Outpatient visits for influenza-like illness (ILI) reported by volunteer sentinel providers and influenza laboratory surveillance data from volunteer sentinel clinical laboratories reported to the California Department of Public Health (CDPH) for the 2015-16 and 2016-17 influenza seasons were available for this study. Sentinel providers (physicians, nurse practitioners, and physician assistants) situated throughout California report on a weekly basis the number of patients seen with influenza-like illness (ILI) and the total number of patients seen for any reason, from which the percentage of provider visits due to ILI can be obtained. ILI is defined as any illness with fever (greater than 37.8°C for oral readings) and cough and/or sore throat in the absence of a known cause other than influenza. Laboratory surveillance for influenza involves the use of data from clinical laboratories throughout California. These laboratories report the number of laboratory-confirmed influenza virus detections and the total number of specimens tested for each virus on a weekly basis, from which the percentage of laboratory tests positive for influenza can be obtained. All data from CDPH were divided into five standard California regions (shown in Figure 2.S2-A and the Supplemental Information) and aggregated by CDC weekending date prior to analysis. Herein, ILI surveillance data refers to the percent of provider visits due to ILI as reported by sentinel providers. Influenza laboratory surveillance refers to the percent of laboratory tests positive for influenza.

Smart Thermometer and Mobile Application Data

The typical Kinsa user is a family with one or more child under the age of 12. Kinsa thermometers are sold in 5,000 retail stores across the country and on Amazon. Anonymized data

from smart thermometers and the corresponding mobile application collected for the 2015-16 and 2016-17 influenza seasons and reported in California were available for this study and is summarized in Figure 2.1. For the purposes of our analysis, season 1 is defined to be Aug. 30, 2015 to Aug. 27, 2016 and season 2 is defined to be Aug. 28, 2016 to Aug. 26, 2017. With each temperature reading, users have the option to specify type of temperature reading--oral, rectal, aural, or underarm--and which user associated with the device took the reading, as well as indicate which of 12 symptoms were present from a preset list of the following: body aches, chills, cough, diarrhea, earache, fatigue, headache, nausea, runny nose, shortness of breath, sore throat, and stomachache. Users also had the option of inputting symptoms without taking a temperature reading. Readings and records were assigned a geolocation based on GPS or IP address and this was used to assign each reading to one of the five CDPH influenza surveillance regions prior to delivery of the dataset. The timestamp for each reading and record was given as a Centers for Disease Control (CDC) weekending date. During seasons 1 and 2, there were 1,120,508 entries, with 1,016,610 temperature readings and 168,564 symptoms reports (readings and symptom reports can be entered contemporaneously or separately). To exclude devices used for testing and devices used for non-ILI related temperature monitoring, devices associated with more than an average rate greater than 500 temperature readings per year were excluded (based on number of readings since the device was initialized), resulting in 1,058,617 entries, with 957,695 temperature readings and 165,440 symptom reports. See Supplemental Information for more details.

Line listed temperature readings and symptom reports from the smart thermometer and mobile application were converted into time series data as follows: Temperature readings were considered fevers if they were $\geq 38.0^{\circ}C$ for rectal and aural readings, $\geq 37.8^{\circ}C$ for oral readings

and readings from unknown body sites, and $\geq 37.2°C$ for underarm readings. Temperature readings outside of the range $34°C$ to $43°C$ were not categorized as fever or non-fever readings (Miller et al. (2018)).

Multiple readings and records from a single user (or device, if user was not specified) for a given week were collapsed into a single reading or record indicating whether a fever or symptom occurred at any point during that week, as defined by the CDC weekending date. Number of temperature readings, fevers, and symptom reports were aggregated by week. We also determined the number of unique users with fever and cough or sore throat at any point during each week, corresponding to the ILI case definition. When unique user profile was not specified, number of unique devices with fever and cough or sore throat at any point during each week was used. If for a given device, user was not consistently entered, the minimum possible number of unique users was assumed.

To simplify the time series symptoms reports data, we used principal component analysis to extract lower dimensional information that can account for the majority of the variance from a high dimensional dataset. Since our objective was to quantify the predictive capability of the temperature readings and symptom reports, principal component analysis was performed on the weekly time series of the number reporting each of the 12 symptoms to reduce the dimensionality of this subset of the data. A priori, we planned to retain only the minimum number of principal components to account for at least 90% of the variance in weekly symptoms reporting.

To account for a growing number of smart thermometer users over time, time series data from the smart thermometers and mobile application were detrended. Detrending was performed

for each region sequentially by fitting a linear model using weekending date as the only predictor and returning the residuals from that fit.

A three-point moving average, referred to as smoothing herein, was applied to the following smart thermometer and mobile application time series data: number of temperature readings, number of fevers, percent of readings indicating fever, number of users meeting the ILI case definition, and principal components extracted from the weekly symptoms data. A three-point moving average was also applied to CDPH influenza surveillance data and ILI surveillance data.

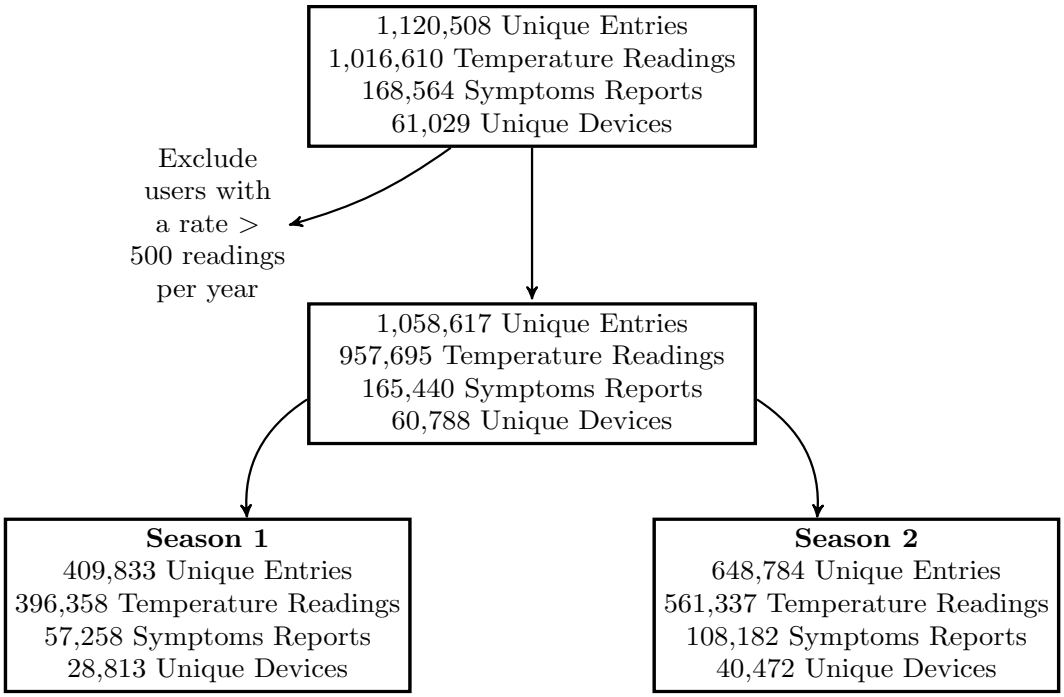

Figure 2.1: Summary of smart thermometer and mobile application data available for seasons 1 and 2 in California. Note that an entry may consist of a temperature reading, reported symptoms, or both. Note that smoothed data, filtered using a 3-point moving average, includes data from the week before season 1 and the week after season 2 in the smoothed time series data within seasons 1 and 2.

Analysis

The aims of our analysis were threefold: First, we aimed to quantify the correlation between time series data from the smart thermometer and mobile application and time series influenza laboratory surveillance data and ILI surveillance data and determine whether these correlations differed across regions. Correlations between smoothed and detrended time series smart thermometer and mobile application data and time series CDPH data for seasons 1 and 2 and all 5 California regions were calculated using the Spearman-rank correlation coefficient. Confidence intervals were determined using the time series bootstrap with a fixed width of 5 (T. S. Rao, Rao, and Rao (2012)). Unsmoothed and raw correlations are presented in the Supplemental Information.

Second, we aimed to determine whether smart thermometer readings and symptom reports in a given region and season were more predictive of CDPH influenza and ILI surveillance data for that region than for other regions or seasons. That is, since influenza patterns are highly correlated across regions in California, high correlations could be indicative of capturing regionally and seasonally independent trends. Therefore, we aimed to ascertain whether smart thermometer readings and symptom reports are correlated with surveillance data because they are reflective of differences in influenza and ILI timing and intensity for the region in which they were recorded. To achieve this aim, smart thermometer and mobile application data were used to predict influenza laboratory surveillance data and ILI surveillance data using a pre-specified time series regression model, with the following regressors: weekending date, total number of users taking temperature readings, total number of users with fevers, percent of users with fever, and the principal components of the symptoms, accounting for at least 90% of the variance in symptoms reporting (see Supplemental Information for further details). Specifically,

we tested the hypothesis that data from a given season and region predicts an outcome for that season and region better than data from other seasons and regions. For each of 10 possible combinations of season and region, smart thermometer and mobile application data were used to predict state regional data for the corresponding week in that season and region combination, as well as the corresponding week in all other season and region combinations. For each model, we estimated an R^2. This yields a 10×10 matrix, whose diagonal elements represent the predictive capability based on modeling using the same season and region. Permutation testing was used to test the hypothesis that the off-diagonal elements were smaller than the diagonal elements. The predictive specificity of the smart thermometer and mobile application was evaluated for both CDPH influenza laboratory surveillance data and CDPH ILI surveillance data. See Supplemental Information for additional details.

Third and finally, we aimed to determine whether the smart thermometer and mobile application data has the potential to improve influenza and ILI predictions. To do this, for each week j in year two, we first developed a model to predict week k of influenza surveillance data, using only the $k-2$ and $k-3$ weeks of influenza surveillance data (to account for realistic reporting delays), as well as flexible functions of time, for all $k < j$. Using elastic net regression, we selected a set of regressors that minimized the squared error for the predictions of week j using regressors determined only from prior times summed over each j (see Supplemental Information for additional details). These regressors were used in a final model. We then evaluated whether including the percentage of users meeting the ILI case definition improved model fit. Specifically, we added a linear term for the change in the percentage of smart thermometer users meeting the ILI case definition determined from the prior and current week, reflecting the fact that smart thermometer and mobile application participant data is available in

realtime. *P*-values and percent decrease in the mean-squared error were determined using time-series bootstrap with a fixed width of 5. Confidence intervals were obtained using the percentile method. A similar procedure was performed for ILI surveillance data.

Results

Smart thermometer and mobile application data change with a temporal pattern mirroring changes in the California influenza and ILI surveillance data (Figure 2.2). After smoothing and detrending, they are strongly correlated with regional CDPH influenza laboratory surveillance data and ILI surveillance data, with Spearman correlation coefficients ranging from 0.79 to 0.91 (Table 1). Detrended fevers are plotted against CDPH influenza and ILI surveillance data for each region in Figure 2.3. The correlations were comparably strong for all regions and for both influenza and ILI. Unsmoothed and raw correlations are also all significantly different from zero and are given in the Supplemental Information. Correlations with other smart thermometer and mobile application time series data is given in the Supplemental Information.

Smoothed thermometer readings and symptom reports were more predictive of smoothed influenza and ILI surveillance data in the same season and region than in others: $p = 0.0032$ and $p = 0.0051$, for influenza and ILI, respectively. We find the first principal component derived from the time series symptoms data explains 96% of the variance. In the first principal component, cough is a very important symptom, followed by runny nose and fatigue; gastrointestinal symptoms are the least important. The loadings of the first four principal components and plots of the time series for the first four principal components are given in the Supplemental Information.

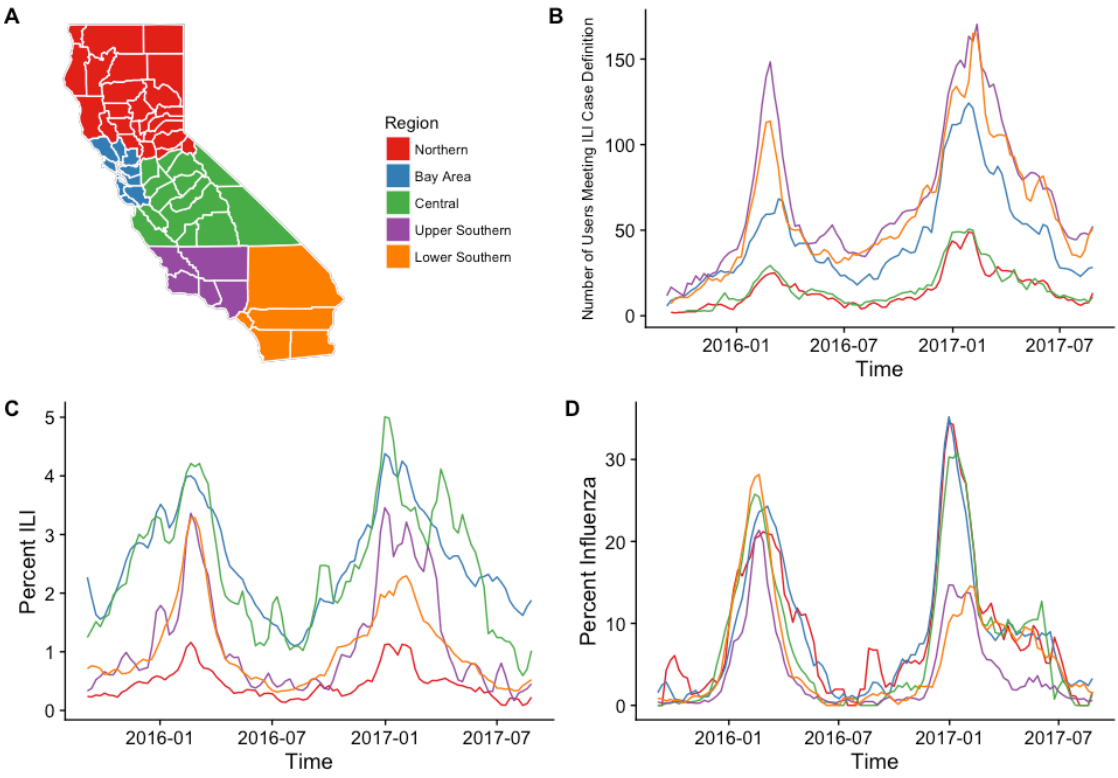

Figure 2.2: Influenza and ILI activity by California region. A: California regions (annotated version in the Supplemental Information). B: Number of individuals with temperature readings and reporting symptoms consistent with the ILI case definition using the smart thermometer and mobile application (not detrended). C: ILI surveillance data (CDPH sentinel provider data). D: Influenza laboratory surveillance data (CDPH laboratory data). All data are smoothed using a three-point moving average.

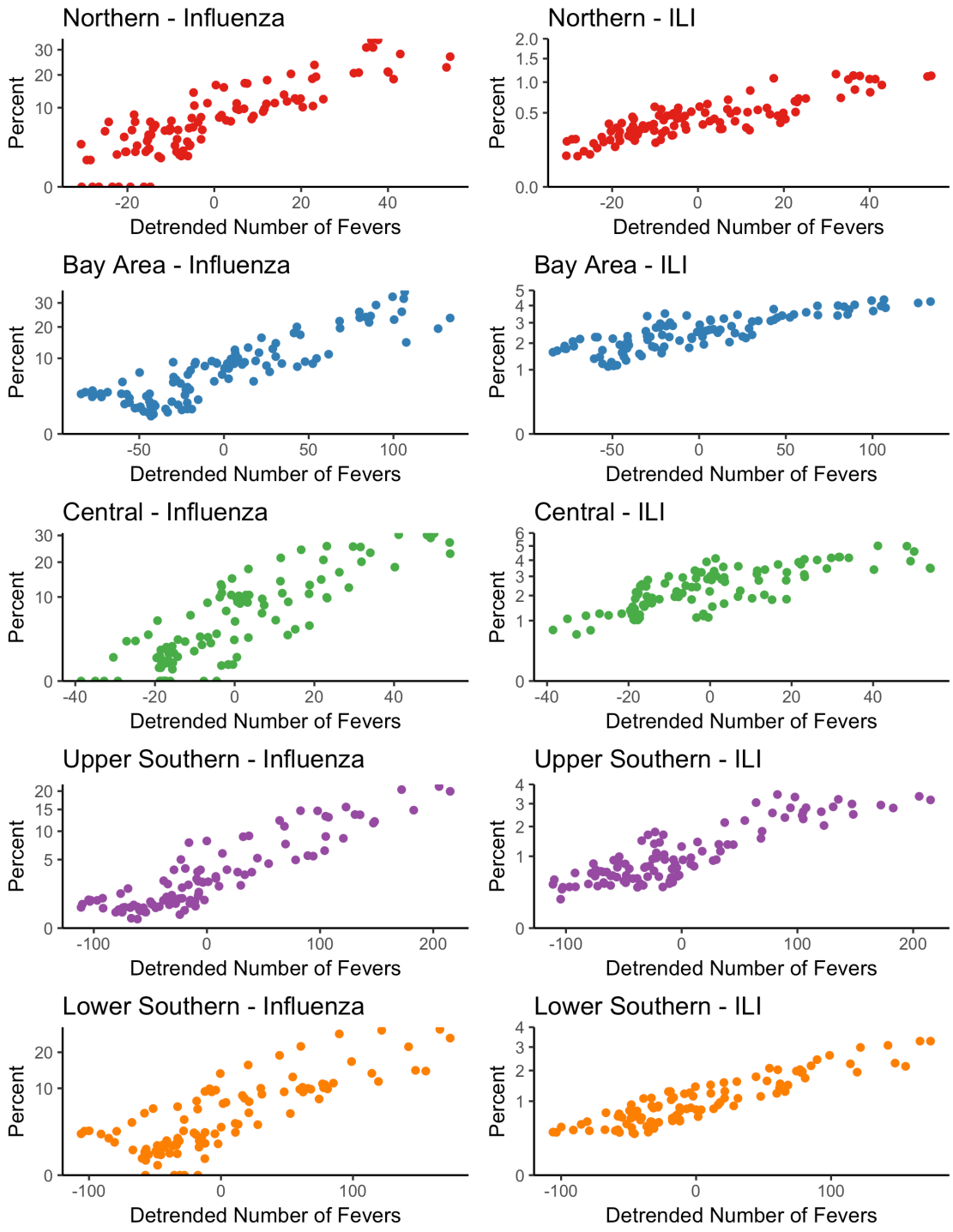

Figure 2.3: Influenza laboratory surveillance data and ILI surveillance data versus detrended number of fevers as reported with the smart thermometer by California region. All values are smoothed using a three-point moving average. For influenza graphs, percents of tests positive for influenza are shown. For ILI graphs, percents of provider visits due to ILI are shown.

	Correlation	Lower Confidence Limit	Upper Confidence Limit	*p*-Value
Northern Influenza	0.88	0.80	0.92	<0.001
Northern ILI	0.87	0.73	0.94	<0.001
Bay Area Influenza	0.88	0.81	0.94	<0.001
Bay Area ILI	0.86	0.71	0.93	<0.001
Central Influenza	0.86	0.72	0.93	<0.001
Central ILI	0.79	0.59	0.89	<0.001
Upper Southern Influenza	0.89	0.78	0.94	<0.001
Upper Southern ILI	0.88	0.78	0.94	<0.001
Lower Southern Influenza	0.82	0.70	0.91	<0.001
Lower Southern ILI	0.91	0.82	0.95	<0.001

Table 2.1: Correlations between smoothed detrended number of fevers from the smart thermometer readings and smoothed influenza laboratory surveillance data and ILI surveillance data by California region. (Correlations for data without smoothing and/or detrending are given in the Supplemental Information.)

For predictions of influenza surveillance data, inclusion of the first difference in percent of users meeting the ILI case definition as a linear predictor in the model improved model fit ($p = 0.0049$), resulting in a 2.1 %, 95 % CI: (0.18 %, 4.9 %), reduction in mean squared error. For predictions of ILI surveillance data, we failed to find evidence that the inclusion of the first difference in percent of users meeting the ILI case definition as a linear predictor in the model improved model fit ($p = 0.39$).

Discussion

We examine smart thermometer readings and symptom reports from a mobile application and their relationship to influenza laboratory surveillance data and ILI surveillance data by California region. Smart thermometer readings and symptom reports are more predictive of influenza and ILI for their own region and season than for other times and places. Furthermore, regional temperature readings from the smart thermometer are highly correlated with reported influenza and ILI and these associations are comparable across California regions. Lastly, these data can be used to improve predictions of regional influenza surveillance data, but not necessarily ILI surveillance data with the model selection procedure we employ. Therefore, these results are consistent with the hypothesis that smart thermometer readings and symptom reports from a mobile application reflect underlying disease transmission and can provide insight into the epidemiology of influenza and ILI in California.

While crowdsourced data lacks the quality assurance and face validity of surveillance data from providers and laboratories (Olson et al. (2013), Cook et al. (2011), Butler (2013)), it may nevertheless provide additional insight on disease transmission dynamics (Santillana et al. (2014)). The realtime availability of such data may aid in prediction and nowcasting efforts (Smith et al. (2016), Preis and Moat (2014)). Influenza is not a reportable disease in California, except for outbreaks, influenza-associated deaths in persons under 65 years of age, and novel influenza infections. Furthermore, testing and reporting practices may vary with seasonal expectations of influenza. For example, there may be less testing and reporting in the late spring, summer, and early fall than in the winter months. Therefore, California influenza laboratory surveillance data and ILI surveillance data may provide an incomplete picture of influenza activity. Participatory surveillance systems have the potential to address gaps in these systems by

bolstering surveillance in regions with fewer participating sentinel providers and laboratories and in young and middle-aged adult populations. In addition, crowdsourced data are available in realtime and may be useful for influenza prediction efforts, particularly with the addition of data from a cloud-based device. Under realistic conditions, there may be delays in obtaining surveillance data, and we find that the addition of smart thermometer and mobile application data can improve predictions of influenza surveillance data. While reductions in the mean-squared error in predictions were not large, influenza follows a predictable seasonal pattern and is autocorrelated, and thus large reductions in error from a single data source can be difficult to achieve (Dugas et al. (2013)). We failed to find evidence that such data could improve ILI predictions made using the model selection procedure we employ and regressing on two prior weeks, however. We do note that at the multi-state level these data were found to improve ILI predictions (Miller et al. (2018)).

The majority of previous participatory surveillance efforts have relied solely on self-reported fevers, in addition to self-reported symptoms (e.g. Chunara et al. (2013)). Our study extends this literature by using temperature readings directly from an FDA-cleared device. Previous studies have illustrated that time series participatory surveillance data is strongly correlated with influenza and ILI surveillance data (e.g. Hswen et al. (2017), Smolinski et al. (2015)) and that data from the Kinsa smart thermometer is correlated with and predictive of ILI at the multi-state level (Miller et al. (2018)). Corroborating such findings, this study suggests that smart thermometer data can provide epidemiologically specific data on regional influenza and ILI activity in California and improve influenza predictions in California.

This study has several limitations. Our analysis pertained to only the two most recent influenza seasons. Thermometers are sold in retail stores throughout the state of California. Nonetheless,

purchasers and users of smart thermometers may not be a representative sample and may not have a uniform geographic distribution. In addition, not all smart thermometer users were necessarily residents of the region for which their data was attributed. Location was determined based on location of reading or report as determined by GPS or IP address, and not region or state of residence. The CDPH surveillance data may also include individuals who traveled outside their region or state of residence, although the probability a sick individual outside of their region or state of residence visited a clinic and/or provided a specimen may differ from the probability that such an individual used a smart thermometer. Since weekending date was the smallest time increment, there may be some error in the estimates of the number of smart thermometer users with fever or meeting the ILI case definition. Our procedure to test the predictive capability of these data aimed to minimize the potential for spurious conclusions due to over or under fitting the data prior to the inclusion of smart thermometer and mobile application data in predictive models. However, to rigorously evaluate the predictive capability of the percent of users meeting the ILI case definition, as well as other channels of this data, predictions of influenza and ILI surveillance data would need to be tested as current surveillance data became available.

Crowdsourced data from mobile applications may contain their own biases (Benke (2017), Lazer et al. (2014)). Nonetheless, crowdsourced data and data from cloud-based devices may provide unique benefits, which may not be available for other data collection methods (Deiner et al. (2016), Deiner, Lietman, and Porco (2017)), such as realtime availability and geoprecision. Furthermore, such data may be particularly useful when it does not rely entirely on self-report, as is the case with smart thermometer readings from an FDA-cleared device. As the user base continues to grow for cloud-based devices, these data will likely continue to provide

epidemiologically specific data on regional influenza and ILI activity in California. These findings may contribute to our understanding of the strengths and weaknesses of big data in epidemiology.

Smart thermometers and mobile applications have the potential to supplement influenza and ILI surveillance systems in regions with a sufficient user base. In addition, realtime data on influenza and ILI are needed to mobilize public health resources in a timely fashion, and crowdsourced data can help address this by nowcasting before CDC reports become available. These data could be used for influenza and ILI prediction efforts at the regional level in California.

Chapter 2 Supplemental Information

California Regions

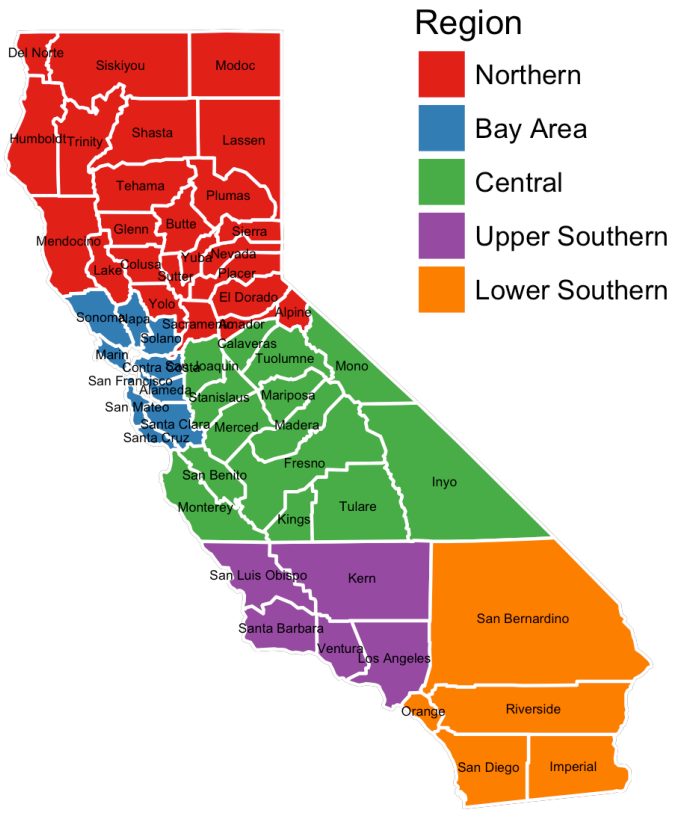

Figure 2.S1: California Regions.

Exclusions

To exclude devices used for testing and devices used for non-ILI related temperature monitoring, devices associated with more than an average rate greater than 500 temperature readings per year were excluded based on number of readings since the device was initialized. We might imagine that a large family with 5 children might have 5 bouts of illness per child per year and that the children's temperatures might be taken 4 times a day over a 5-day period. This would result in

500 readings for such a device per year and might be considered a reasonable upper bound for the rate of temperature readings for a device used for influenza and ILI monitoring.

Pre-specified Model

The pre-specified model includes the following predictors for the kth region and season combination from the smart thermometer and mobile application: weekending date t, total number of readings r_k, number of fevers f_k, percent of readings indicating fever p_k, and the first principal component of the symptoms data c_k. Data from the smart thermometer and mobile application from the kth region and season combination is used to predict the outcome for the ith season and region combination Y_i, where the outcome is either influenza laboratory surveillance data or ILI surveillance data. All linear terms of the predictors are included, as well as the interactions with weekending date t to account for changes in the user base over time. The model is as follows:

$$E[Y_i] = \beta_0 + \beta_1 r_k + \beta_2 r_k t + \beta_3 f_k + \beta_4 f_k t + \beta_5 p_k + \beta_6 p_k t + \beta_7 c_k + \beta_8 c_k t + \beta_9 t$$

.

Principal Components

	PC1	PC2	PC3	PC4
Body aches	0.2610207	-0.1343484	0.1322127	-0.0135420
Chills	0.2937175	-0.3982687	-0.2061293	-0.1607322
Cough	0.4958834	0.1420079	-0.7423604	0.3253080
Diarrhea	0.0688524	-0.0952334	0.1327917	0.2257187
Ear ache	0.0707892	-0.0574796	0.0175156	0.1274458
Fatigue	0.4465816	-0.4849380	0.1323798	-0.4251842
Headache	0.3006756	-0.0128744	0.3696410	0.0237678
Nausea	0.1269430	-0.0876612	0.2567750	0.4041942
Runny nose	0.4280712	0.7266518	0.2072444	-0.2915332
Short breath	0.0812824	-0.0184077	0.0087004	-0.0133844
Sore throat	0.2731326	0.1012027	0.2027605	0.1444651
Stomach ache	0.1397761	-0.0957822	0.2583816	0.5917810

Table 2.S1: Principal components. Loadings for the first four principal components. PC is used to abbreviate principal component.

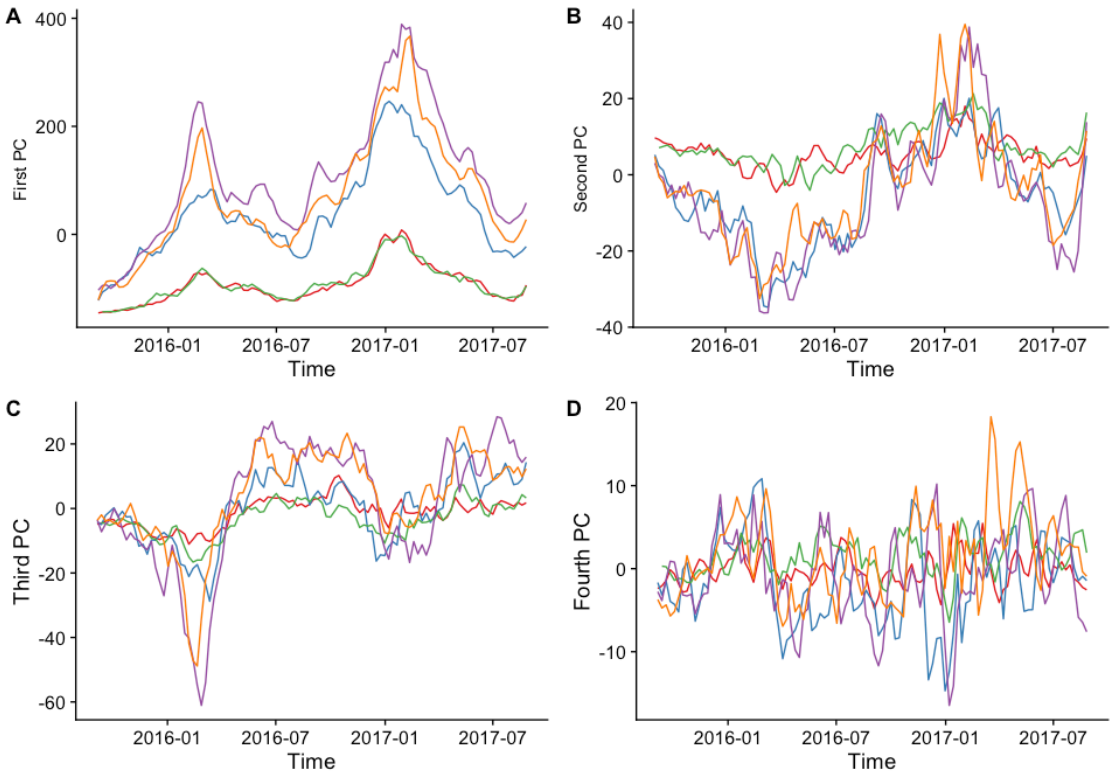

Figure 2.S2: First four principal components of the symptoms data for the five California regions over two influenza seasons. A three-point moving average filter is applied to each component. PC is used to abbreviate principal component. A: First principal component. B: Second principal component. C: Third principal component. D: Fourth principal component. The first four principal components account for 96%, 1.4%, 1.2%, and 0.27% of the total variance, respectively.

Correlations with Unfiltered, Detrended Number of Fevers

We present the correlation coefficients and correlation plots for data without the three-point moving average applied. Number of fevers are detrended to account for an increasing number of users over time. All correlations are significant and comparable across regions.

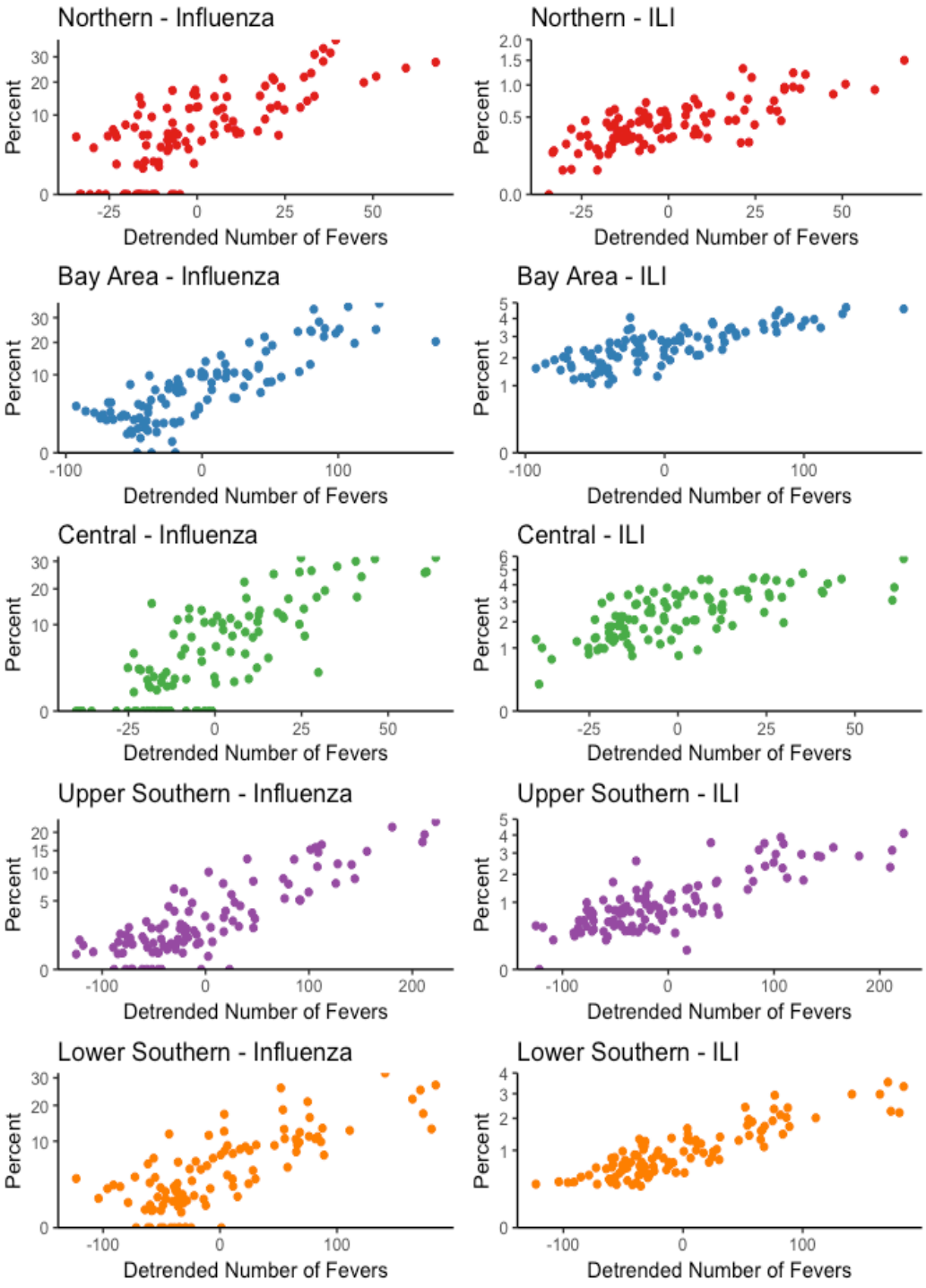

Figure 2.S3: Influenza laboratory surveillance data and ILI surveillance data versus detrended number of fevers as reported with the smart thermometer by California region. For influenza graphs, percents of tests positive for influenza are shown. For ILI graphs, percents of provider visits due to ILI are shown.

	Correlation	Lower Confidence Limit	Upper Confidence Limit	*p*-Value
Northern Influenza	0.79	0.62	0.86	<0.001
Northern ILI	0.78	0.58	0.87	<0.001
Bay Area Influenza	0.85	0.77	0.91	<0.001
Bay Area ILI	0.82	0.63	0.90	<0.001
Central Influenza	0.81	0.61	0.90	<0.001
Central ILI	0.72	0.50	0.84	<0.001
Upper Southern Influenza	0.86	0.67	0.92	<0.001
Upper Southern ILI	0.82	0.66	0.89	<0.001
Lower Southern Influenza	0.80	0.64	0.89	<0.001
Lower Southern ILI	0.88	0.78	0.93	<0.001

Table 2.S2: Correlations between detrended number of fevers from the smart thermometer readings and influenza laboratory surveillance data and ILI surveillance data by California region.

Correlations with Raw Number of Fevers

We present the correlation coefficients and correlation plots for the raw data. All correlations are significant and comparable across regions.

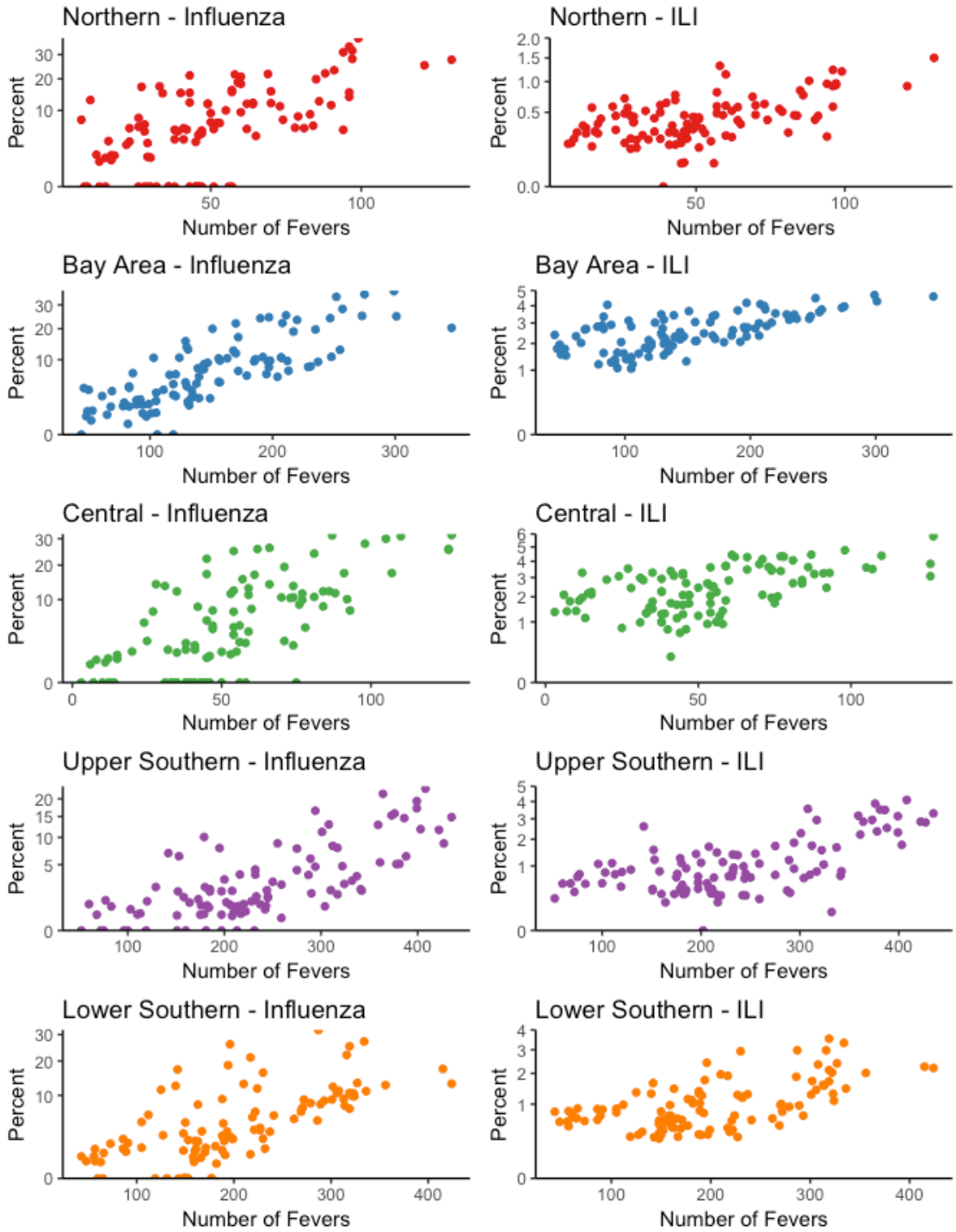

Figure 2.S4: Influenza laboratory surveillance data and ILI surveillance data versus raw number of fevers as reported with the smart thermometer by California region. For influenza graphs, percents of tests positive for influenza are shown. For ILI graphs, percents of provider visits due to ILI are shown.

	Correlation	Lower Confidence Limit	Upper Confidence Limit	*p*-Value
Northern Influenza	0.67	0.39	0.80	<0.001
Northern ILI	0.59	0.29	0.77	<0.001
Bay Area Influenza	0.78	0.63	0.87	<0.001
Bay Area ILI	0.69	0.38	0.85	<0.001
Central Influenza	0.70	0.41	0.84	<0.001
Central ILI	0.56	0.29	0.72	<0.001
Upper Southern Influenza	0.68	0.47	0.81	<0.001
Upper Southern ILI	0.67	0.39	0.81	<0.001
Lower Southern Influenza	0.60	0.41	0.84	<0.001
Lower Southern ILI	0.60	0.36	0.76	<0.001

Table 2.S3: Correlations between raw number of fevers from the smart thermometer readings and influenza laboratory surveillance data and ILI surveillance data by California region.

Correlations with Total Number of Readings

We present the correlation coefficients and correlation plots for total number of unique users taking temperature readings. All correlations are significant and comparable across regions.

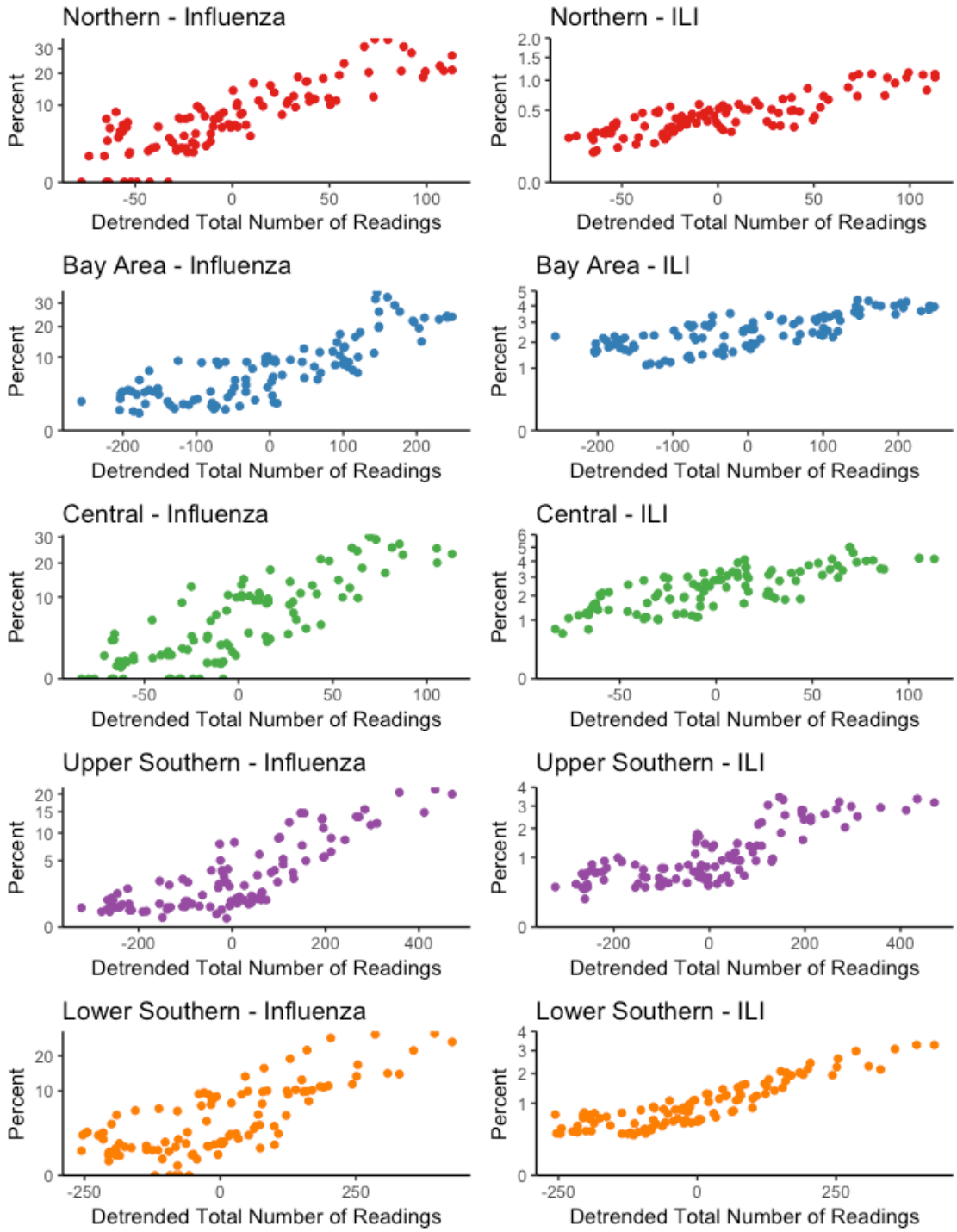

Figure 2.S5: Influenza laboratory surveillance data and ILI surveillance data versus detrended number of readings as reported with the smart thermometer by California region. All values are smoothed using a three-point moving average. For influenza graphs, percents of tests positive for influenza are shown. For ILI graphs, percents of provider visits due to ILI are shown.

	Correlation	Lower Confidence Limit	Upper Confidence Limit	*p*-Value
Northern Influenza	0.86	0.78	0.91	<0.001
Northern ILI	0.86	0.69	0.93	<0.001
Bay Area Influenza	0.79	0.69	0.89	<0.001
Bay Area ILI	0.77	0.61	0.88	<0.001
Central Influenza	0.82	0.69	0.90	<0.001
Central ILI	0.80	0.64	0.89	<0.001
Upper Southern Influenza	0.80	0.60	0.89	<0.001
Upper Southern ILI	0.80	0.64	0.89	<0.001
Lower Southern Influenza	0.77	0.59	0.87	<0.001
Lower Southern ILI	0.89	0.80	0.95	<0.001

Table 2.S4: Correlations between detrended number of readings from the smart thermometer readings and influenza laboratory surveillance data and ILI surveillance data by California region. All values are filtered using a three-point moving average.

Correlations with Number Meeting ILI Case Definition

We present the correlation coefficients and correlation plots for the number of unique users meeting the ILI case definition. All correlations are significant and comparable across regions.

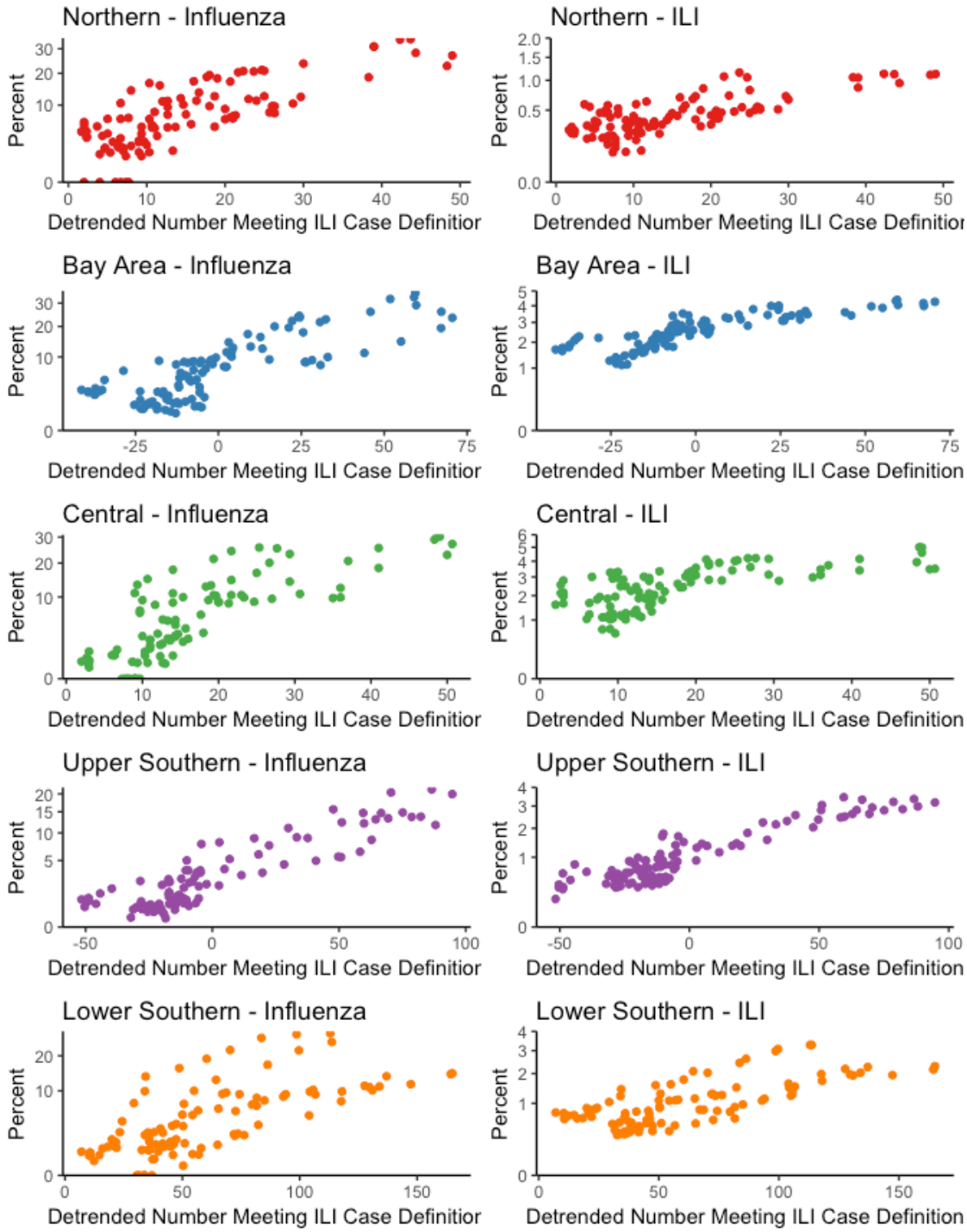

Figure 2.S6: Influenza laboratory surveillance data and ILI surveillance data versus detrended number of users meeting the ILI case definition as reported with the smart thermometer by California region. All values are smoothed using a three-point moving average. For influenza graphs, percents of tests positive for influenza are shown. For ILI graphs, percents of provider visits due to ILI are shown.

	Correlation	Lower Confidence Limit	Upper Confidence Limit	*p*-Value
Northern Influenza	0.83	0.62	0.91	<0.001
Northern ILI	0.79	0.50	0.90	<0.001
Bay Area Influenza	0.84	0.70	0.93	<0.001
Bay Area ILI	0.86	0.78	0.93	<0.001
Central Influenza	0.84	0.64	0.94	<0.001
Central ILI	0.72	0.53	0.84	<0.001
Upper Southern Influenza	0.90	0.80	0.95	<0.001
Upper Southern ILI	0.94	0.87	0.97	<0.001
Lower Southern Influenza	0.65	0.49	0.89	<0.001
Lower Southern ILI	0.73	0.57	0.87	<0.001

Table 2.S5: Correlations between detrended number of smart thermometer users meeting the ILI case definition in a given week and influenza laboratory surveillance data and ILI surveillance data by California region. All values are filtered using a three-point moving average.

Correlations with Percent of Fever Readings

We present the correlation coefficients and correlation plots for the percent of users with fever.

All correlations and comparable across regions.

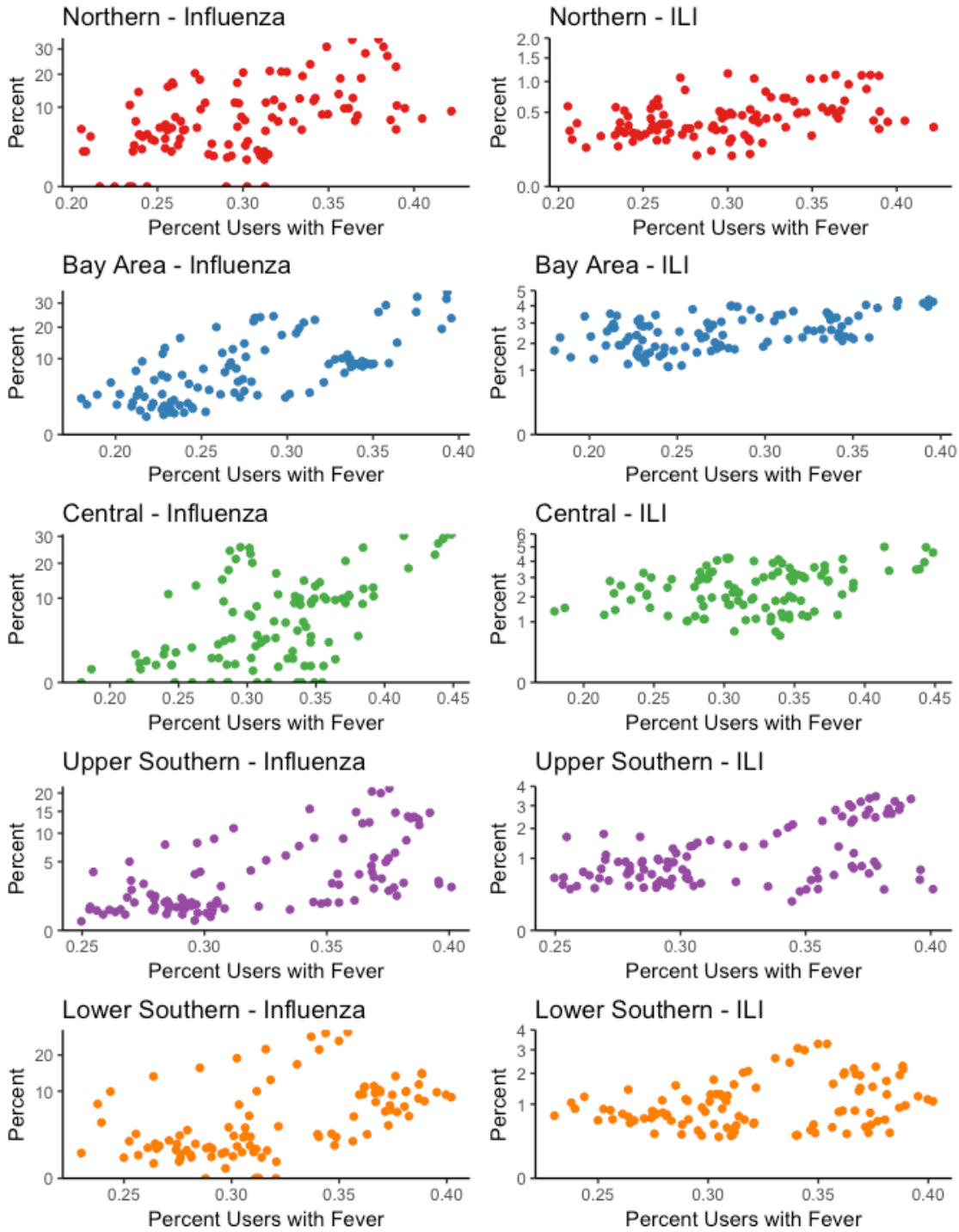

Figure 2.S7: Influenza laboratory surveillance data and ILI surveillance data versus percent of smart thermometer readings indicating fever by California region. All values are smoothed using a three-point moving average. For influenza graphs, percents of tests positive for influenza are shown. For ILI graphs, percents of provider visits due to ILI are shown.

	Correlation	Lower Confidence Limit	Upper Confidence Limit	*p*-Value
Northern Influenza	0.50	0.24	0.72	<0.001
Northern ILI	0.41	0.09	0.68	0.02
Bay Area Influenza	0.65	0.35	0.82	<0.001
Bay Area ILI	0.52	0.16	0.76	0.01
Central Influenza	0.54	0.14	0.77	0.02
Central ILI	0.36	-0.04	0.63	0.08
Upper Southern Influenza	0.55	0.31	0.76	<0.001
Upper Southern ILI	0.54	0.15	0.80	0.01
Lower Southern Influenza	0.43	0.22	0.78	<0.001
Lower Southern ILI	0.32	0.03	0.58	0.03

Table 2.S6: Correlations between percent of smart thermometer readings indicating fever and influenza laboratory surveillance data and ILI surveillance data by California region. All values are filtered using a three-point moving average.

Correlations with First Principal Component of Symptoms Data

We present the correlation coefficients and correlation plots for the first principal component of the symptoms data. All correlations are significant and comparable across regions.

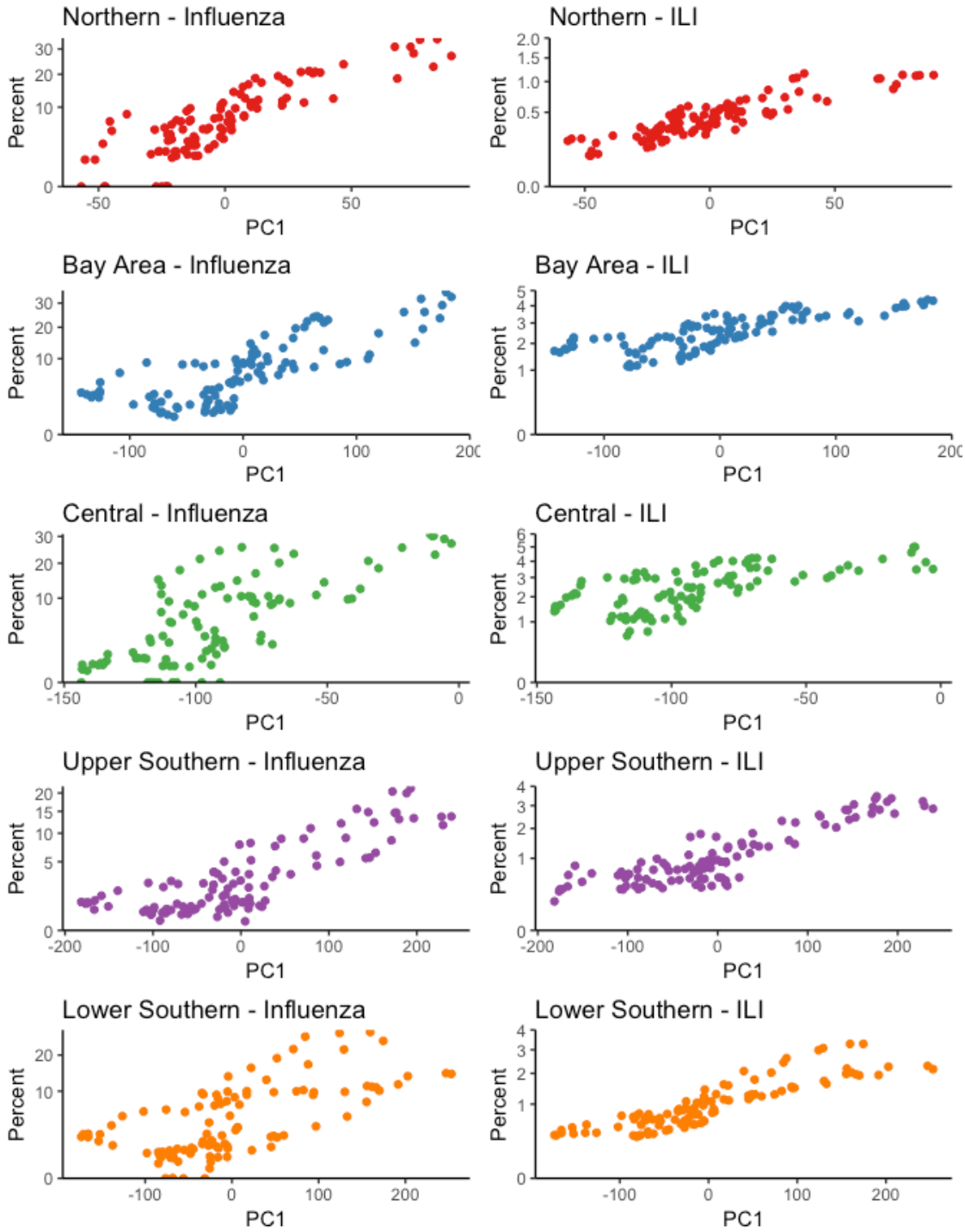

Figure 2.S8: Influenza laboratory surveillance data and ILI surveillance data versus detrended first principal component of the symptoms data as reported with the mobile application by California region. All values are smoothed using a three-point moving average. For influenza graphs, percents of tests positive for influenza are shown. For ILI graphs, percents of provider visits due to ILI are shown.

	Correlation	Lower Confidence Limit	Upper Confidence Limit	*p*-Value
Northern Influenza	0.89	0.77	0.95	<0.001
Northern ILI	0.90	0.79	0.95	<0.001
Bay Area Influenza	0.81	0.64	0.90	<0.001
Bay Area ILI	0.81	0.66	0.90	<0.001
Central Influenza	0.77	0.48	0.91	<0.001
Central ILI	0.69	0.49	0.82	<0.001
Upper Southern Influenza	0.81	0.68	0.90	<0.001
Upper Southern ILI	0.89	0.73	0.94	<0.001
Lower Southern Influenza	0.65	0.50	0.80	<0.001
Lower Southern ILI	0.86	0.81	0.94	<0.001

Table 2.S7: Correlations between the detrended first principal component of the symptoms data and influenza laboratory surveillance data and ILI surveillance data by California region. All values are filtered using a three-point moving average.

Predicting Influenza and ILI

To evaluate the ability of smart thermometer data to improve predictions of influenza and ILI surveillance data, we performed the model selection procedure described in the methods. For each week j in year two, we regressed the outcome of interest for week k using the outcome for the weeks $k-2$ and $k-3$, week number (linear predictor), weeks since start of season 1 (linear predictor), and a number of flexible functions of time of the form $\sin(n(2\pi k/52.2 - 2m\pi/8))$ for $n = 1/2$, 1, 2, and 3 and $m = 0,1,2,..,6,7$ for all $k < j$. The coefficients for these predictors were then used to predict week j for each region. Elastic net regression was used to find the predictors that the minimized the total mean squared error of the predictions of j week using coefficients estimated from prior weeks summed over region and week j in year 2. If multiple functions of time with the same n were selected, the linear combination was used as a predictor, weighted by the respective regression coefficients using both full years of data. These predictors were then used to determine whether the addition of the change in ILI as determined by the smart thermometer application improved model fits for prediction of week k using the set of predictors determined by elastic net regression. For predictions of influenza surveillance data, the selected predictors were influenza surveillance data for 2 weeks prior, and sine terms with $n = 1$, 2, and 3. For predictions of ILI surveillance data, the selected predictors were ILI surveillance data for 2 and 3 weeks prior and sine terms with $n = 1$ and 2.

Chapter 3

School-Based Varicella Transmission in California: Insights from Branching Processes

Introduction

Varicella is a highly contagious disease transmitted by direct contact with an infectious individual and aerosols, and while severe disease is rare in children, varicella can result in complications, including death (McKinney and others (2011), Heininger and Seward (2006)). Contact investigation for varicella can be both challenging and expensive (Leung et al. (2015)). Thus, efforts to decrease disease burden have focused on vaccination of school-aged and younger children. Beginning in 1996, the Advisory Committee on Immunization Practices (ACIP) recommended a single dose of varicella vaccine for children in the United States (Leung et al. (2015)). A single dose was not found to be sufficient to prevent school-based outbreaks and, in some outbreaks, a majority of cases were among singly vaccinated children (Lopez et al. (2006)). In 2007, the ACIP revised and updated its recommendations for varicella vaccination, recommending two doses, as well as recommending a catchup dose for children who previously received only one dose (Leung et al. (2015), Marin et al. (2007)). In post-licensure studies, two doses of varicella vaccine were 98% effective at preventing any form of varicella compared with approximately 84% effectiveness with only one dose (Shapiro et al. (2011), Kuter et al. (2004)). California school entry requirements were updated in 2017 to require two doses of varicella vaccine prior to school entry.

Varicella transmission is endemic in the United States, likely due at least in part to a reservoir of infection from adults who develop zoster (shingles) (Ferguson, Anderson, and

Garnett (1996)). However, it is not known whether transmission is self-limited among children in school-based settings (Leung et al. (2015)). School-based outbreaks of varicella would likely begin with a child who obtained varicella from another infectious individual with a primary infection (e.g. a child at another school) or an adult with zoster (e.g. a caregiver) (Ferguson, Anderson, and Garnett (1996)). School-based outbreaks in California are only reported if they reach a final size of 5 or greater, and other states have similar reporting practices (Leung et al. (2015)).

We analyze school-based varicella outbreaks reported to the California Department of Public Health during 2006–2015 with the aim of determining whether the reproduction number of varicella changed following the ACIP revised recommendations. Previously, it has been found that the shift to two-dose scheduling was associated with a decrease in the number, size, and duration of varicella outbreaks in nine states, including school-based outbreaks (Leung et al. (2015)). While in other settings finite observed outbreak sizes within a defined geographic region might reasonably imply subcritical transmission, finite outbreak sizes within a school could be indicative of subcritical transmission or a supercritical process with infection occurring across multiple schools. We use branching process theory to gain insight into the expected distributions of outbreak sizes and durations for four plausible regimes of within-school transmission: a subcritical process, a supercritical process for which we have observed only self-limited outbreaks, a supercritical process with depletion of susceptibles, and a process that begins as supercritical, but for which transmission declines during an outbreak.

Methods

California varicella outbreak surveillance data from 2006 through 2015 were included in this analysis. Varicella outbreaks were defined as five or more cases clustering in time and place. Outbreak analysis were restricted to school settings.

All analysis was performed in R 3.3.0. The Kruskal-Wallis rank sum test was used to determine to test whether the median size and duration differed for at least one year from other years. Two-sided permutation testing with 1024 replicates was used to evaluate for a significant trend in outbreak sizes and durations. Bootstrapped confidence intervals with 1024 replicates were used to calculate the 95% confidence limits for rate of change in size and duration. The Wilcoxon signed rank test was used to test for differences of medians of outbreak size and duration in 2006 and 2007 (pre-policy change) compared with outbreak sizes and durations for 2008-2015 and 2008-2013 (post-policy change), respectively.

For the first part of the branching process analysis, we assumed a Galton-Watson branching process with a negative binomial secondary case distribution with two parameters: a reproduction number R, which gives the mean of the secondary case distribution, and a dispersion parameter k. $k = 1$ corresponds to a geometric distribution, $k < 1$ represents an overdispersed distribution relative to the geometric, and as k approaches infinity, the secondary case distribution approaches a Poisson distribution. Equations and methods described in previous publications (S. F. Ackley et al. (2017), Blumberg et al. (2014), S. Blumberg and Lloyd-Smith (2013), Blumberg, Funk, and Pulliam (2014), Lloyd-Smith (2007), Lloyd-Smith, Schreiber, and Getz (2006)). Previous work on measles has shown that the secondary case distribution may be overdispersed compared with a geometric distribution ($k < 1$) (Ackley et al. (2017), Blumberg et al. (2014), Blumberg and Lloyd-Smith (2013)). Assuming subcritical transmission within

schools, we estimate a reproduction number R from the distribution of outbreak sizes conditional on outbreak size greater than five (Ackley et al. (2017), Blumberg et al. (2014), Blumberg et al. (2015)). We use the following recursive relationship to describe the cumulative probability F of extinction in g generations, which is then used to obtain a mean number of generations as a function of R and k: $F_{g+1} = \sum_{s=0}^{\infty} p_s \, (F_g)^s$, where p_s gives the probability of a single case producing s cases. For the purposes of numerically determining the cumulative probability of extinction in g generations F_g, the above summation was performed for s from 1 to 10,000.

Outbreaks are reported conditional on size 5 or greater. To determine the effect of conditioning on size, we conditioned on specific sizes to determine how R and heterogeneity in R affect the outbreak duration. This heterogeneity could either be due to over-dispersion, described using k, or due to declining transmissibility with each generation; we define a parameter α, which is the relative mean reproduction number with each increasing generation. To calculate the expected number of generations conditional on a specific outbreak size n, we first enumerated all possible transmission networks for that size. Then, to determine the probability that an outbreak of size n is of a specific total number of generations g, we summed over each possible configuration that produced a number of total generations g the product of the probabilities that the number of cases in each generation producing the number of cases in the subsequent generation for that configuration, with 0 cases in the $g + 1$ generation.

For a supercritical process characterized by depletion of susceptibles, we calculate the final size distribution of an SEIR process assuming a gamma-distributed infectious period using a recursion as described elsewhere (Demiris et al. (2006), Bailey (1953), Bailey (1975)).

Results

A summary of California school-based outbreaks for 2006-2015 is shown in Figure 3.1. Figure 3.2 shows the number of school-based outbreaks of size 5 or greater, the number of individuals in these outbreaks, and the number of California hospitalizations in children (18 and under) by year. The number of outbreaks decreases from over 100 in 2006 per year to under 10 per year following 2010.

We examined the data for evidence of changes in the distribution of outbreak sizes and durations over time. We find evidence that the median size is not the same for all 10 years ($p = 0.04$), but fail to find evidence that the median duration differed for any of the 10 years ($p = 0.85$). In a trend test, we find an average change in size of -0.67 people per year, 95% CI (-1.14, -0.19), which is highly significant ($p = 0.004$). We estimate an average change in duration of -0.71 days per year, 95% CI (-2.05, 0.74), but this change is not significant ($p = 0.47$). The median size is significantly decreased following 2007 ($p = 0.0004$), but we fail to find evidence of change in duration ($p = 0.4$). If we assume subcritical transmission within schools and a single index case, we estimate a reproduction number R from the distribution of outbreak sizes. The observed sizes for 2006 and 2007 corrrespond to an estimate of R of 0.74, 95% CI (0.71, 0.76), and following 2007, the observed sizes correspond to an estimate of R of 0.65, 95% CI (0.45,0.71).

Hospitalizations in children due to varicella remained roughly constant over the 2010-2015 time period. However, the ratio of the number of individuals in reported school-based outbreaks to the number of hospitalizations decreased by -1.43, 95% CI (-3.27, -0.09) and this change is significant ($p = 0.04$). However, this result is highly senstive to underreporting of

outbreaks in later years. If, for example, two outbreaks of size 5 were not reported in each 2014 and 2015, the change in this ratio would be similar, but not statistically significant ($p = 0.08$). As shown in Figure 3.3, our analysis of a Galton-Watson branching process unconditional on size indicates that for reproduction numbers less than unity, both mean outbreak size and duration decrease with decreasing R. For reproduction numbers greater than unity, mean outbreak size and duration decrease with increasing R for finite sized outbreaks. However, the extinction probability also decreases with increasing R.

Figures 3.4 and 3.5 show the effect R and k (Figure 3.4) or α (Figure 3.5) on outbreak duration after conditioning on a single, specific outbreak size. Conditional on a single, specific size, we obtain no additional information about the mean R for an outbreak from the outbreak durations. However, the durations may yield information about transmission heterogeneity. While k and α describe two very different types of heterogeneity, they have a similar effect on duration conditional on size, as shown in Figures 3.4-A and 3.5.

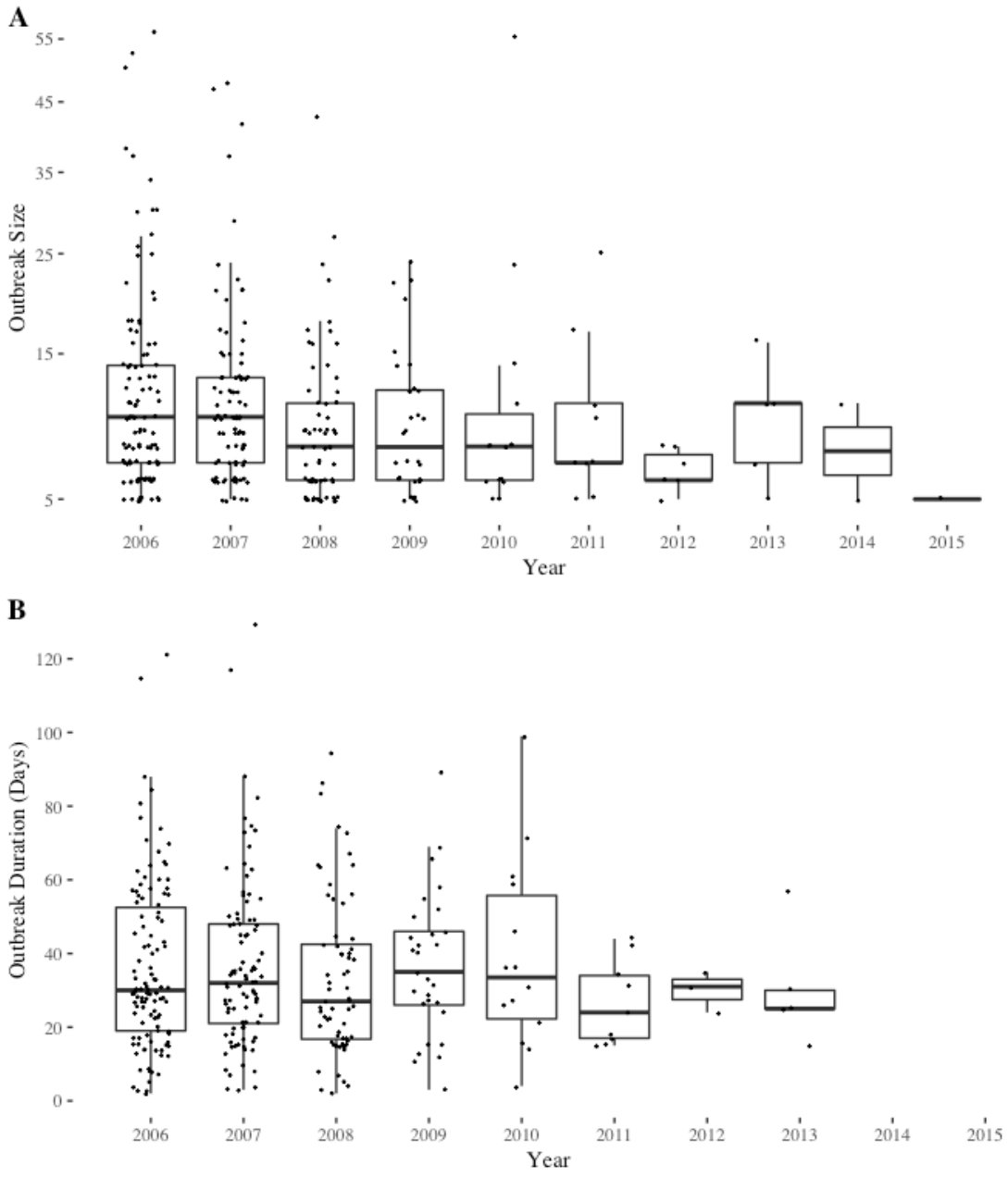

Figure 3.1: Box plots of school-based outbreak sizes (top) and durations (bottom) by year in California. All sizes and durations are shown as overlaid points.

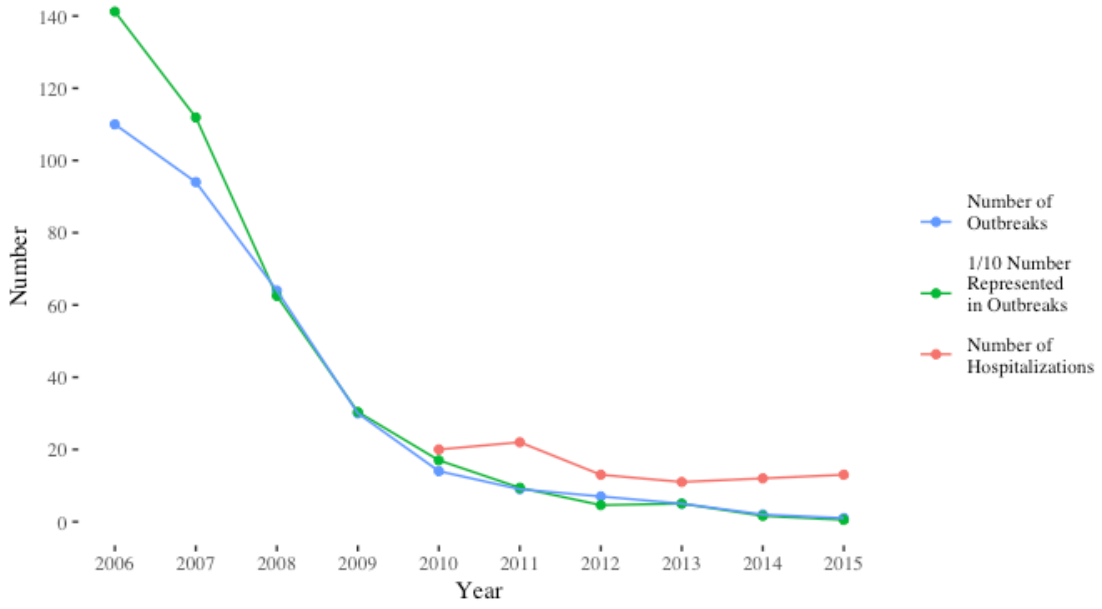

Figure 3.2: Number of school-based outbreaks of size 5 or greater, number of individuals represented in outbreaks, and number of hospitalizations in children by year.

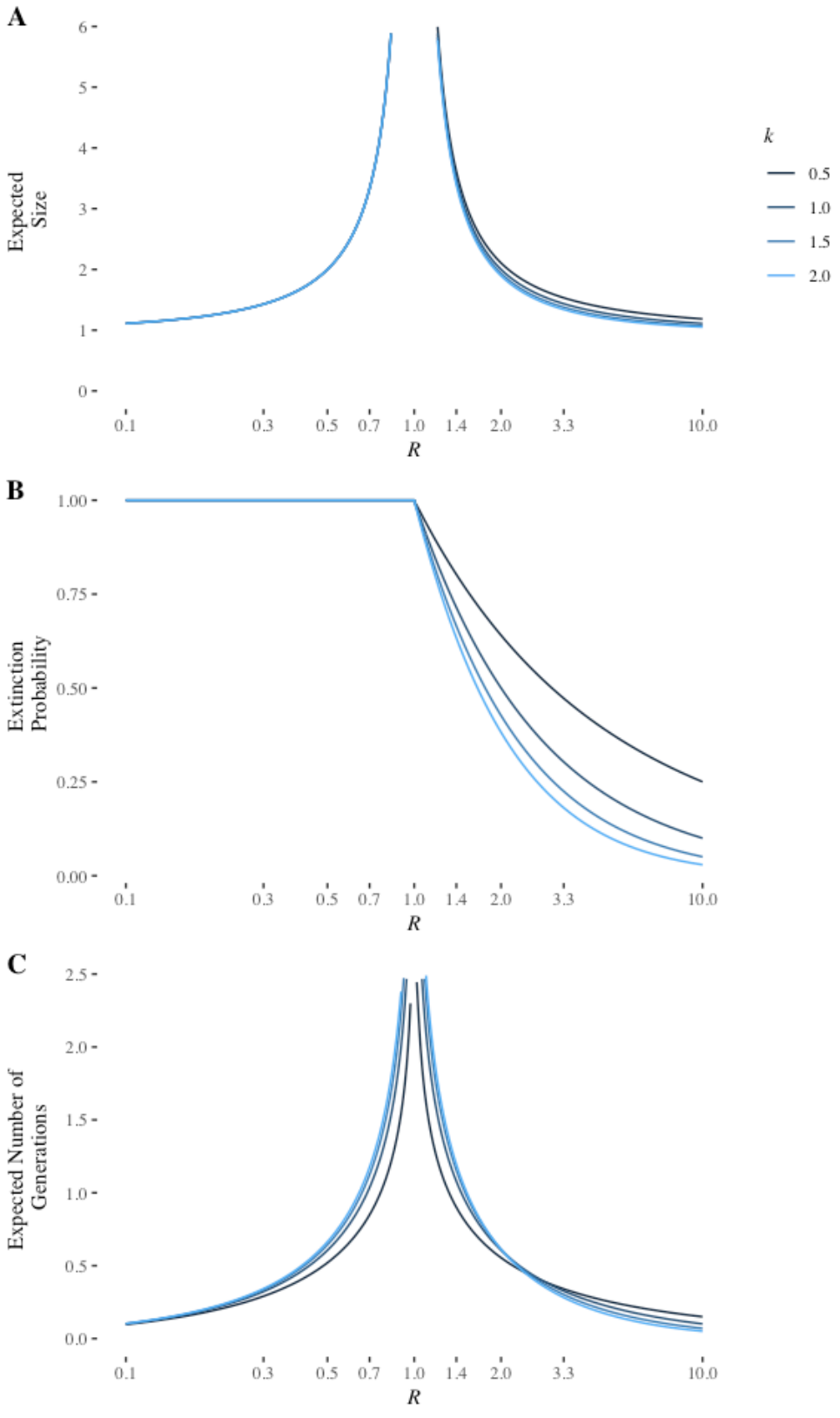
A
Expected Size
6
5
4
3
2
1
0
0.1
0.3
0.5
0.7
1.0
1.4
2.0
3.3
10.0
R
k
0.5
1.0
1.5
2.0
B
Extinction Probability
1.00
0.75
0.50
0.25
0.00
0.1
0.3
0.5
0.7
1.0
1.4
2.0
3.3
10.0
R
C
Expected Number of Generations
2.5
2.0
1.5
1.0
0.5
0.0
0.1
0.3
0.5
0.7
1.0
1.4
2.0
3.3
10.0
R

Figure 3.3: Expected sizes, extinction probabilities, and number of generations for a Galton-Watson branching process model. A: Expected size as a function of the reproduction number R, and for various values of the dispersion parameter k, conditional on extinction. B: Extinction probability as a function of R and for various values of k. C: Expected number of generations as a function of the reproduction number R, and for various values of the dispersion parameter k, conditional on extinction. Note lower values of k correspond with a zero-inflated, overdispersed secondary case distribution and may be more realistic (Ackley et al. (2017), Lloyd-Smith, Schreiber, and Getz (2006)).

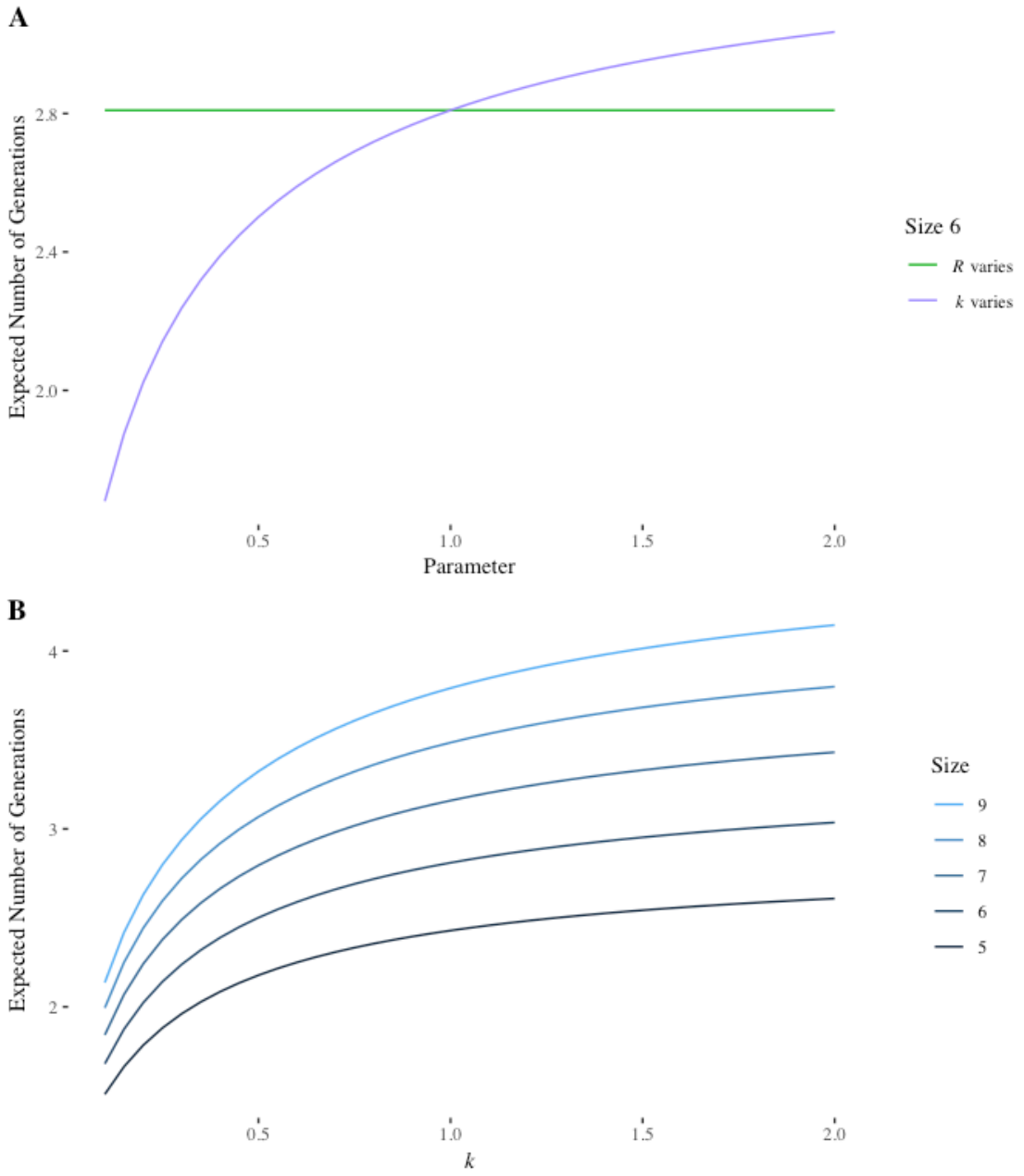

Figure 3.4: The effect of R and k on outbreak duration conditional on outbreak size. A: Conditional on size 6, the expected number of generations in an outbreak does not depend on R, but does depend on k. Not only does the expected number of generations not depend on R, but the distribution of the number of generations is also independent of R. B: Expected number of generations as a function of k conditional on sizes 5 to 9.

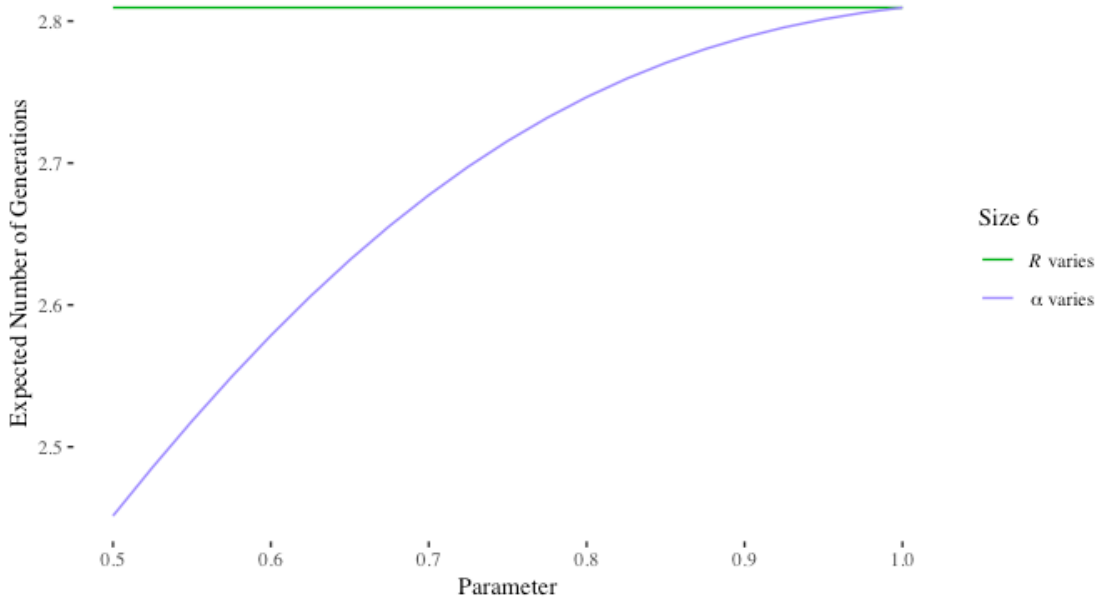

Figure 3.5: The effect of R and α on outbreak duration conditional on outbreak size. Conditional on size 6, the expected number of generations in an outbreak does not depend on the mean R, but does depend on α.

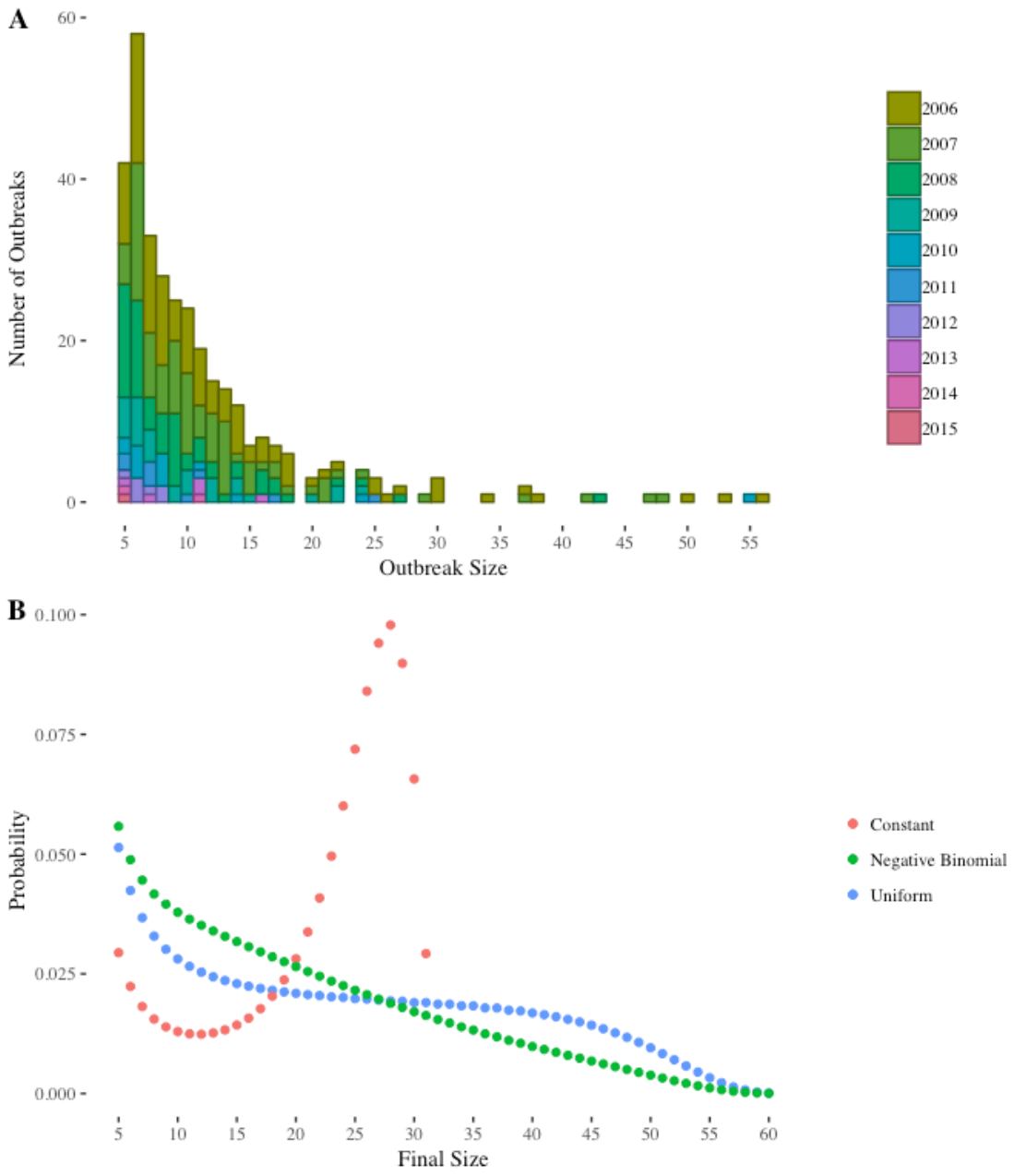

Figure 3.6: The observed distribution of outbreak sizes and theoretical distribution of outbreak sizes for a supercritical process. **A:** The overall observed distribution of outbreak sizes and by year. Following size 6, the number of outbreaks declines with increasing size. **B:** The distribution of outbreak sizes for sizes of 5 or greater for a supercritical SEIR process with $R = 2$ and an exponentially-distributed serial interval. If the number of susceptibles per school is constant, the most probable outbreak sizes are just shy of this number of susceptibles However, if there is heterogeneity in the number of susceptibles per school, the distribution of outbreak sizes may be monotonically decreasing, similar to what is observed in A.

Discussion

Following the change in ACIP recommendations for varicella vaccination in 2007, the median outbreak size decreased. However, while the number of outbreaks has continued to decrease following 2008, we do not find evidence that the distribution of sizes has changed since 2008. We do not find evidence for changes in the distribution of outbreak durations over time. We evaluated the plausibility of three possible scenarios for varicella transmission in schools: a subcritical process, a supercritical process without depletion of susceptibles, and a supercritical process with declining transmissibility, due to depletion of susceptibles or other factors. Under realistic conditions, all of these scenarios can produce a monotonically decreasing distribution of outbreak sizes, similar to the observed distribution of outbreak sizes. For supercritical varicella transmission in a single school with a constant number of susceptibles, this distribution of outbreak sizes is not monotonically decreasing, peaking just below the maximum possible size. However, if we assume schools have differing numbers of susceptibles, as is more realistic, it is possible to obtain a monotonically decreasing distribution (see Figure 3.4). Thus, we cannot conclude that school-based transmission of varicella is subcritical based on the distribution of outbreak sizes conditional on size five or greater.

Based on other sources of information, we may be able to argue that one of these scenarios is more plausible than another. For a supercritical branching process (no depletion of susceptibles) finite outbreak sizes are only observed when the process goes extinct. For reproduction numbers just above unity and with small dispersion parameters (a secondary case distribution overdispersed compared with a geometric distribution), extinction can be quite probable, over 90%. However, even with a very high extinction probability, over 100 outbreaks were reported in each 2006 and 2007 each. Therefore, we would argue that either depletion of

susceptibles plays an essential role in limiting outbreak sizes or that outbreaks are self-limiting due to a subcritical reproduction number.

While we cannot exclude the possibility of supercritical transmission, especially in 2006 and 2007, the data following 2007 is consistent with a process that became subcritical in school-based settings in 2008. Theoretical work has shown that for a subcritical disease with a constant reproduction number less than unity the prevalence will decrease over time, but the distribution of prevalences across homologous geographic regions conditional on a non-zero prevalence is approximately the same when prevalences are low (Worden et al. (2017), Nåsell (1996)). Following 2007, we see a significant decline in the outbreak size and some evidence for a change in the distribution of outbreak sizes. However, we did not find evidence that the distribution of outbreak sizes changed following this, but the number of school-based outbreaks continued to decline. This is consistent with a subcritical process within the school resulting in less community transmission and thus fewer introductions of cases into school settings.

In this analysis, we were restricted to outbreaks of size five or greater. With a reproduction number less than unity, the unconditional outbreak size and duration should decrease for as the reproduction decreases (see Figure 3.2). However, by semi-conditioning on size, we diminish our ability to track changes in size and duration as the reproduction number changes. We find that fully conditioning on size yields a distribution of number of generations that is independent of the reproduction number, but not the dispersion parameter. We also note that changes in the dispersion parameter can affect the expected sizes and durations of outbreaks. This has the potential to make changes in outbreak sizes and durations over time—or a lack thereof—difficult to interpret. For example, we did not find evidence of a decrease in duration or a change in the distribution of durations over this time period, which would be consistent both

with a constant R and k or an increasing k and declining R. We note that significant declines in duration are seen in other states over this time period, and may be indicative of a declining R (Leung et al. (2015)).

Reporting smaller varicella outbreaks would allow us to better discern changes in outbreak size or duration over time resulting from changes in the reproduction number. However, there may be limitations to such a strategy. Outbreaks of size five or greater have high specificity for varicella; for singletons or outbreaks of size two to four, misdiagnosis or misreporting would be more likely and could make discerning real changes in the distribution of outbreak sizes or durations difficult or impossible. Furthermore, irrespective of regime, we might expect to see a monotonically decreasing distribution of outbreak sizes that depends both on the reproduction number and the dispersion parameter of the secondary case distribution.

A measure that might help discern changes in the reproduction number over time, rather than just a continued decline in prevalence, would be the ratio of cases represented in outbreaks of size five or greater to a reasonable proxy for total cases, such as number hospitalizations due to varicella or its complications. If varicella were supercritical in school-based settings, a large proportion of cases would be represented in outbreaks size five or greater, whereas for a subcritical process a very small fraction of cases would be represented in outbreaks of size five or greater. We do find that following 2010 the number of cases represented in school-based outbreaks declines relative to hospitalizations. This may indicate a continued decline in transmissibility following 2010, or may indicate recent underreporting of school-based outbreaks.

Our results indicate that a reduction in the number of outbreaks and changes in outbreak size and outbreak duration are not necessarily clear indicators of changes in transmissibility or

susceptibility to disease. With the new, more effective shingles vaccine Shingrix available starting in 2017 (Tsui and Cohen (2018)) there may be even fewer introductions of varicella into school settings if vaccine uptake is high. Understanding how observed distributions of outbreak sizes and durations change with changing transmissibility will aid in disentangling the effects of the new vaccine and potential continued declines in transmissibility.

References

Chapter 1

Bailey, N. T. J. 1953. "The total size of a general stochastic epidemic," *Biometrika*, 40 (1): 177–185.

Bartlett, M. S. 1960. "The critical community size for measles in the United States," *Journal of the Royal Statistical Society*. Series A (General), 123 (1): 37–44.

Blumberg, S., W. T. A. Enanoria, J. O. Lloyd-Smith, T. M. Lietman, and T. C. Porco. 2014. "Identifying postelimination trends for the introduction and transmissibility of measles in the United States," *American Journal of Epidemiology*.

Blumberg, S., W. Enanoria, and T. C. Porco. 2015. "Vaccination compliance and the US measles epidemic," *JAMA Pediatrics*, 169 (9): 877–877.

Blumberg, S., S. Funk, and J. R. C. Pulliam. 2014. "Detecting differential transmissibilities that affect the size of self-limited outbreaks," *PLoS Pathogens*, 10 (10).

Blumberg, S. and J. O. Lloyd-Smith. 2013. "Comparing methods for estimating R_0 from the size distribution of subcritical transmission chains," *Epidemics*, 5 (3): 131–145.

Blumberg S. and J. O. Lloyd-Smith. 2013. "Inference of R_0 and transmission heterogeneity from the size distribution of stuttering chains," *PLoS Computational Biology*, 9 (5).

Blumberg, S., L. Worden, W. Enanoria, S. Ackley, M. Deiner, F. Liu, D. Gao, T. Lietman, and T. C. Porco. 2015. "Assessing measles transmission in the United States following a large

outbreak in California," *PLoS Currents*, 7.

Coughlin, M. M., A. S. Beck, B. Bankamp, and P. A. Rota. 2017. "Perspective on global measles epidemiology and control and the role of novel vaccination strategies," *Viruses*, 9(1); 11.

Dayan, G. H., I. R. Ortega-Sanchez, C. W. LeBaron, M. P. Quinlisk, and Iowa Measles Response Team. 2005. "The cost of containing one case of measles: The economic impact on the public health infrastructure—Iowa, 2004," *Pediatrics*, 116 (1).

El Mubarak, H. S., S. Yuksel, G. van Amerongen, P. G. Mulder, M. M. Mukhtar, A. D. Osterhaus, and R. L. de Swart. 2007. "Infection of cynomolgus macaques (*Macaca fascicularis*) and rhesus macaques (*Macaca mulatta*) with different wild-type measles viruses," *Journal of General Virology*, 88 (7): 2028–2034.

Farrington, C. P., M. N. Kanaan, and N. J. Gay. 2003. "Branching process models for surveillance of infectious diseases controlled by mass vaccination," *Biostatistics*, 4 (2): 279–295.

Fiebelkorn, A. P., S. B. Redd, K. Gallagher, P. A. Rota, J. Rota, W. Bellini, and J. Seward. 2010. "Measles in the United States during the postelimination era," *Journal of Infectious Diseases*, 202 (10): 1520–1528.

Fine, P. E. M., and J. A. Clarkson. 1982. "Measles in England and Wales: An analysis of factors underlying seasonal patterns," *International Journal of Epidemiology*, 11 (1): 5–14.

Fitzmaurice, G. M., N. M. Laird, and J. H. Ware. 2012. *Applied Longitudinal Analysis*. John Wiley & Sons.

Grenfell, B. T. 1992. "Chance and chaos in measles dynamics," *Journal of the Royal Statistical*

Society. Series B (Methodological), 54 (2): 383–398.

Harris, T. E. 1989. *The Theory of Branching Processes*. Dover Publications, Inc.

Katz, S. L., C. A. De Quadros, H. Izurieta, L. Venczel, and P. Carrasco. 2004 "Measles eradication in the Americas: Progress to date," *Journal of Infectious Diseases*, 189 (1): S227–S235.

Liu, F., W. T. Enanoria, J. Zipprich, S. Blumberg, K. Harriman, S. F. Ackley, W. D. Wheaton, J. L. Allpress, and T. C. Porco. 2015. "The role of vaccination coverage, individual behaviors, and the public health response in the control of measles epidemics: An agent- based simulation for California," *BMC Public Health*, 15 (1): 447.

Lloyd-Smith, J. O., S. J. Schreiber, and W. M. Getz. 2005. "Moving beyond averages: Individual- level variation in disease transmission," *Contemporary Mathematics*, 410: 209–234.

Majumder, M. S., Cohn EL, Mekaru S. R., Huston J. E., and Brownstein J. S. 2015. "Substandard vaccination compliance and the 2015 measles outbreak," *JAMA Pediatrics*, 169 (5): 494–495.

Measles | Cases and Outbreaks | CDC. [Online]. Available: https://www.cdc.gov/measles/cases-outbreaks.html

——. 1957. "Measles periodicity and community size," *Journal of the Royal Statistical Society*. Series A (General), 120 (1): 48–70.

Mello, M. M., D. M. Studdert, and W. E. Parmet. 2015. "Shifting vaccination politics the end of personal-belief exemptions in California," *New England Journal of Medicine*, 373 (9): 785–787.

Mikolajczyk, R., M. Akmatov, S. Rastin, and M. Kretzschmar. 2008. "Social contacts of school children and the transmission of respiratory-spread pathogens," *Epidemiology and Infection*, 136 (6): 813–822.

Nishiura, H., P. Yan, C. K. Sleeman, and C. J. Mode. 2012. "Estimating the transmission potential of supercritical processes based on the final size distribution of minor outbreaks," *Journal of Theoretical Biology*, 294: 48–55.

Nuzzo R. 2015. "Fooling ourselves," *Nature*, 526 (7572): 182–185.

Orenstein, W. A., K. L. Samuel, and A. R. Hinman. 2004. "Summary and conclusions: Measles elimination meeting, 16–17 March 2000," *Journal of Infectious Diseases*, 189 (1): S43–S47.

Ortega-Sanchez, I. R., M. Vijayaraghavan, A. E. Barskey, and G. S. Wallace. 2014. "The economic burden of sixteen measles outbreaks on United States public health departments in 2011," *Vaccine*, 32 (11): 1311–1317.

Rota, P. A., K. Brown, A. Mankertz, S. Santibanez, S. Shulga, C. P. Muller, J. M. Hubschen, M. Siqueira, J. Beirnes, H. Ahmed et al. 2011, "Global distribution of measles genotypes and measles molecular epidemiology," *Journal of Infectious Diseases*, 204 (1): S514–S523.

Rota, P. A., W. J. Moss, M. Takeda, R. L. de Swart, K. M. Thompson, and J. L. Goodson. 2016. "Measles," *Nature Reviews*. Disease Primers, 2: 16049.

Scherer A., and A. McLean. 2002. "Mathematical models of vaccination," *British Medical Bulletin*, 62 (1): 187–199.

Surveillance Manual | Measles | Vaccine Preventable Diseases | CDC. [Online]. Available:

http://www.cdc.gov/vaccines/pubs/surv-manual/chpt07-measles.html

Sugerman, D. E., A. E. Barskey, M. G. Delea, I. R. Ortega-Sanchez, D. Bi, K. J. Ralston, P. A. Rota, K. Waters-Montijo, and C. W. LeBaron. 2010. "Measles outbreak in a highly vaccinated population, San Diego, 2008: role of the intentionally undervaccinated," *Pediatrics*, 125 (4): 747–755.

World Health Organization et al. 2012. "Measles virus nomenclature update: 2012," *Weekly Epidemiological Record*, 87 (9): 73–81.

Zipprich, J., K. Winter, J. Hacker, D. Xia, J. Watt, K. Harriman et al. 2015. "Measles outbreak: California, December 2014–February 2015," *Morbidity and Mortality Weekly Report*, 64 (6): 153–154.

Chapter 2

Benke, K. K. 2017. "Uncertainties in Big Data When Using Internet Surveillance Tools and Social Media for Determining Patterns in Disease Incidence." *JAMA Ophthalmology*, 135 (4): 402–2.

Biggerstaff, M., D. Alper, M. Dredze, S. Fox, I. C. Fung, K. S. Hickmann, B. Lewis, et al. 2016. "Results from the Centers for Disease Control and Prevention's Predict the 2013–2014 Influenza Season Challenge." *BMC Infectious Diseases*, 16 (1): 357.

Butler, D. 2013. "When Google Got Flu Wrong." *Nature*, 494 (7436): 155.

Chunara, R., S. Aman, M. Smolinski, and J. S. Brownstein. 2013. "Flu Near You: An Online Self-Reported Influenza Surveillance System in the Usa." *Online Journal of Public Health Informatics*, 5 (1).

Cook, S., C. Conrad, A. L. Fowlkes, and M. H. Mohebbi. 2011. "Assessing Google Flu Trends Performance in the United States During the 2009 Influenza Virus a (H1n1) Pandemic." *PloS One*, 6 (8).

Deiner, M. S., T. M. Lietman, and T. C. Porco. 2017. "Uncertainties in Big Data When Using Internet Surveillance Tools and Social Media for Determining Patterns in Disease Incidence–Reply." *Jama Ophthalmology*, 135 (4): 402–3.

Deiner, M. S., T. M. Lietman, S. D. McLeod, J. Chodosh, and T. C. Porco. 2016. "Surveillance Tools Emerging from Search Engines and Social Media Data for Determining Eye Disease Patterns." *JAMA Ophthalmology*, 134 (9): 1024–30.

Dugas, A. F., M. Jalalpour, Y. Gel, S. Levin, F. Torcaso, T. Igusa, and R. E. Rothman. 2013. "Influenza Forecasting with Google Flu Trends." *PloS One*, 8 (2).

Hswen, Y., S. S. Brownstein, J. Liu, and J. B. Hawkins. 2017. "Use of a Digital Health Application for Influenza Surveillance in China." *American Journal of Public Health*, 107(7):1130-6.

Lampos, V., A. C. Miller, S. Crossan, and C. Stefansen. 2015. "Advances in Nowcasting Influenza-Like Illness Rates Using Search Query Logs." *Scientific Reports*, 5.

Lazer, D., R. Kennedy, G. King, and A. Vespignani. 2014. "The Parable of Google Flu: Traps in Big Data Analysis." *Science*, 343 (6176). American Association for the Advancement of Science: 1203–5.

Marquet, R. L., A. I. M. Bartelds, S. P. van Noort, C. E. Koppeschaar, J. Paget, F. G. Schellevis, and J. van der Zee. 2006. "Internet-Based Monitoring of Influenza-Like Illness (ILI) in the General Population of the Netherlands During the 2003–2004 Influenza Season." *BMC Public Health*, 6 (1): 242.

Miller, A. C., I. Singh, E. Koehler, and P. M. Polgreen. 2018. "A Smartphone-Driven Thermometer Application for Real-Time Population-and Individual-Level Influenza Surveillance." *Clinical Infectious Diseases*.

Olson, D. R., K. J. Konty, M. Paladini, C. Viboud, and L. Simonsen. 2013. "Reassessing Google Flu Trends Data for Detection of Seasonal and Pandemic Influenza: A Comparative Epidemiological Study at Three Geographic Scales." *PLoS Computational Biology*, 9 (10).

Ortiz, J. R., H. Zhou, D. K. Shay, K. M. Neuzil, A. L. Fowlkes, and C. H. Goss. 2011. "Monitoring Influenza Activity in the United States: A Comparison of Traditional Surveillance Systems with Google Flu Trends." *PloS One*, 6 (4).

Preis, T., and H. S. Moat. 2014. "Adaptive Nowcasting of Influenza Outbreaks Using Google Searches." *Royal Society Open Science*, 1 (2): 140095.

Rao, T. S., S. S. Rao, and C. R. Rao. 2012. *Time Series Analysis: Methods and Applications*. Vol. 30.

Santillana, M., D. W. Zhang, M. M. Althouse, and J. W. Ayers. 2014. "What Can Digital Disease Detection Learn from (an External Revision to) Google Flu Trends?" *American Journal of Preventive Medicine*, 47 (3): 341–47.

Smith, M., D. A. Broniatowski, M. J. Paul, and M. Dredze. 2016. "Towards Real-Time Measurement of Public Epidemic Awareness: Monitoring Influenza Awareness Through Twitter." In *AAAI Spring Symposium on Observational Studies Through Social Media and Other Human-Generated Content*.

Smolinski, M. S., A. W. Crawley, K. Baltrusaitis, R. Chunara, J. M. Olsen, O. Wójcik, M. Santillana, A. Nguyen, and J. S. Brownstein. 2015. "Flu Near You: Crowdsourced Symptom Reporting Spanning 2 Influenza Seasons." *American Journal of Public Health*, 105 (10): 2124–30.

Wójcik, O. P., J. S. Brownstein, R. Chunara, and M. A. Johansson. 2014. "Public Health for the People: Participatory Infectious Disease Surveillance in the Digital Age." *Emerging Themes in Epidemiology*, 11 (1): 7.

Chapter 3

Ackley, S. F., J. K. Hacker, W. T. A. Enanoria, L. Worden, S. Blumberg, T. C. Porco, and J. Zipprich. 2017. "Genotype-Specific Measles Transmissibility: A Branching Process Analysis." *Clinical Infectious Diseases*, 66 (8): 1270–5.

Bailey, N. T. J. 1953. "The Total Size of a General Stochastic Epidemic." *Biometrika*. 177–85.

Bailey, N. T. J. 1975. *The Mathematical Theory of Infectious Diseases and Its Applications*. Charles Griffin & Company Ltd, 5a Crendon Street, High Wycombe, Bucks HP13 6LE.

Blumberg, S., and J. O. Lloyd-Smith. 2013. "Comparing Methods for Estimating R0 from the Size Distribution of Subcritical Transmission Chains." *Epidemics*, 5 (3): 131–45.

Blumberg, S., W. T. A. Enanoria, J. O. Lloyd-Smith, T. M. Lietman, and T. C. Porco. 2014. "Identifying Postelimination Trends for the Introduction and Transmissibility of Measles in the United States." *American Journal of Epidemiology*, 179 (11): 1375–82.

Blumberg, S., S. Funk, and J. R. C. Pulliam. 2014. "Detecting Differential Transmissibilities That Affect the Size of Self-Limited Outbreaks." *PLoS Pathogens*, 10 (10).

Blumberg, S., L. Worden, W. Enanoria, S. Ackley, M. Deiner, F. Liu, D. Gao, T. Lietman, and T. C. Porco. 2015. "Assessing Measles Transmission in the United States Following a Large Outbreak in California." *PLoS Currents*, 7.

Demiris, N., and P. D. O'Neill. 2006. "Computation of Final Outcome Probabilities for the Generalised Stochastic Epidemic." *Statistics and Computing*, 16 (3): 309–17.

Ferguson, N. M., R. M. Anderson, and G. P. Garnett. 1996. “Mass Vaccination to Control Chickenpox: The Influence of Zoster.” *Proceedings of the National Academy of Sciences*, 93 (14): 7231–5.

Heininger, U., and F. F. Seward. 2006. “Varicella.” *The Lancet*, 368 (9544): 1365–76.

Kuter, B., H. Matthews, H. Shinefield, S. Black, P. Dennehy, B. Watson, K. Reisinger, et al. 2004. “Ten Year Follow-up of Healthy Children Who Received One or Two Injections of Varicella Vaccine.” *The Pediatric Infectious Disease Journal*, 23 (2): 132–37.

Leung, J., A. S. Lopez, J. Blostein, N. Thayer, J. Zipprich, A. Clayton, V. Buttery, et al. 2015. “Impact of the US Two-Dose Varicella Vaccination Program on the Epidemiology of Varicella Outbreaks: Data from 9 States, 2005–2012.” *The Pediatric Infectious Disease Journal*, 34 (10): 1105–9.

Lloyd-Smith, J. O. 2007. “Maximum Likelihood Estimation of the Negative Binomial Dispersion Parameter for Highly Overdispersed Data, with Applications to Infectious Diseases.” *PloS One*, 2 (2).

Lloyd-Smith, J. O., S. J. Schreiber, and W. M. Getz. 2006. “Moving Beyond Averages: Individual-Level Variation in.” In *Mathematical Studies on Human Disease Dynamics: Emerging Paradigms and Challenges: AMS-Ims-Siam Joint Summer Research Conference on Modeling the Dynamics of Human Diseases: Emerging Paradigms and Challenges, July 17-21, 2005, Snowbird, Utah*, 410:235. American Mathematical Soc.

Lopez, A. S., D. Guris, L. Zimmerman, L. Gladden, T. Moore, D. T. Haselow, V. N. Loparev, D. S. Schmid, A. O. Jumaan, and S. L. Snow. 2006. "One Dose of Varicella Vaccine Does Not Prevent School Outbreaks: Is It Time for a Second Dose?" *Pediatrics*, 117 (6).

Marin, M., D. Güris, S. S. Chaves, S. Schmid, J. F. Seward, and Advisory Committee on Immunization Practices, Centers for Disease Control and Prevention (CDC). 2007. "Prevention of Varicella: Recommendations of the Advisory Committee on Immunization Practices (ACIP)." *Morbidity and Mortality Weekly Report. Recommendations and Reports*, 56 (RR-4): 1–40.

McKinney, M., and others. 2011. *Lippincott's Guide to Infectious Diseases*. Lippincott Williams & Wilkins.

Nåsell, I. 1996. "The Quasi-Stationary Distribution of the Closed Endemic Sis Model." *Advances in Applied Probability*, 28 (3): 895–932.

Shapiro, E. D., M. Vazquez, D. Esposito, N. Holabird, S. P. Steinberg, J. Dziura, P. S. LaRussa, and A. A. Gershon. 2011. "Effectiveness of 2 Doses of Varicella Vaccine in Children." *The Journal of Infectious Diseases*, 203 (3): 312–15.

Tsui, E., and E. J. Cohen. 2018. "The Importance of Vaccination Against Herpes Zoster." *Current Ophthalmology Reports*, 1–8.

Worden, L., I. B. Schwartz, S. Bianco, S. F. Ackley, T. M. Lietman, and T. C. Porco. 2017. "Hamiltonian Analysis of Subcritical Stochastic Epidemic Dynamics." *Computational and Mathematical Methods in Medicine*.

Publishing Agreement

It is the policy of the University to encourage the distribution of all theses, dissertations, and manuscripts. Copies of all UCSF theses, dissertations, and manuscripts will be routed to the library via the Graduate Division. The library will make all theses, dissertations, and manuscripts accessible to the public and will preserve these to the best of their abilities, in perpetuity.

I hereby grant permission to the Graduate Division of the University of California, San Francisco to release copies of my thesis, dissertation, or manuscript to the Campus Library to provide access and preservation, in whole or in part, in perpetuity.

Author Signature 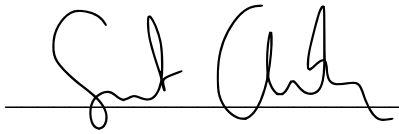 Date October 20, 2018